

# Journal of Mechanics of Materials and Structures

**TIME-ADAPTIVE FINITE ELEMENT SIMULATIONS OF DYNAMICAL  
PROBLEMS FOR TEMPERATURE-DEPENDENT MATERIALS**

Matthias Grafenhorst, Joachim Rang and Stefan Hartmann

**Volume 12, No. 1**

**January 2017**



# TIME-ADAPTIVE FINITE ELEMENT SIMULATIONS OF DYNAMICAL PROBLEMS FOR TEMPERATURE-DEPENDENT MATERIALS

MATTHIAS GRAFENHORST, JOACHIM RANG AND STEFAN HARTMANN

Dynamical systems in finite elements yield systems of second-order differential equations. Incorporating inelastic material properties, thermomechanical coupling and particular Dirichlet boundary conditions essentially changes the underlying mathematical problem. In this respect, we investigate the behavior of a number of subproblems such as reaction force computation, high-order time-integration, time-adaptivity, etc., which yield (depending on the underlying problem) systems of differential-algebraic equations or a mixture of systems of second-order and first-order ordinary differential equations (especially if the constitutive equations are of evolutionary-type, as in the case of viscoelasticity and viscoplasticity). The main goals are to provide higher-order time integration schemes using diagonally implicit Runge–Kutta methods and the generalized- $\alpha$  method so that they may be applied to the constitutive equations, and to apply time-adaptivity via embedded schemes so that step-sizes are chosen automatically. The constitutive equations are given by a thermoviscoplasticity model of Perzyna/Chaboche-type with nonlinear kinematic hardening.

## 1. Introduction

The modeling of thermomechanically coupled material properties is an important and challenging task for both constitutive modeling and for numerical treatment. In the case of polymers, small temperature variations essentially change the mechanical response. Cyclic processes induce heat and must be considered under such circumstances. Other applications are metal forming processes either via heat treatment or by recurrent processes.

The numerical treatment of thermomechanically coupled problems using finite elements is connected to the historical evolution of considering the constitutive equations of rate-type for both quasistatic computations and in the case of dynamical situations. To begin with, let us discuss quasistatic mechanical but transient thermal problems where the constitutive equations are defined by evolution equations of rate-type. The unsteady heat equation yields after its spatial discretization using finite elements to a system of ordinary differential equations (ODEs), which is coupled with the algebraic equations defining the mechanical equilibrium [Lewis et al. 1996; Reddy and Gartling 2000; Quint et al. 2011]. The latter is coupled with the constitutive model of rate-type. In our case, it forms a first-order ODE system as well (with case distinction in the case of viscoplasticity with yield function). This system can be solved using partitioned or monolithic approaches [Schrefler 2004]. In [Felippa and Park 1980; Felippa et al. 2001], the authors proposed a partitioned approach where the mechanical and the thermal parts are solved separately (commonly two different programs and/or meshes are chosen [Erbs and Düster 2012; Erbs et al. 2015; Wendt et al. 2015]). Particular investigations on partitioned systems and their stability

*Keywords:* dynamics, DIRK methods, finite elements, generalized-alpha method, time-adaptivity, thermoviscoplasticity.

are provided in [Simo and Miehe 1992; Armero and Simo 1992; 1993]. The monolithic approach was proposed in [Glaser 1991; Miehe 1988] and extended to high-order time-integration schemes in [Quint 2012; Rothe 2015; Rothe et al. 2015a]. In the latter case, the resulting equations define differential-algebraic equations (DAE) after spatial discretization, using finite elements that lead to changes in the numerical and theoretical properties of the mathematical model. In view of thermoviscoelasticity and the combination of high-order methods in space and time, we refer to [Netz and Hartmann 2015; Hamkar 2013].

Concerning inertia effects, the case of linear elastodynamics for small strains represents a huge scientific area which is not discussed here, as we focus on proposals treating inelastic material properties. The case of finite strain viscoelasticity is treated in [Conde Martín et al. 2014], where the constitutive model must have a particular structure (a so-called GENERIC scheme) to fit within the numerical scheme. This is extended in [Krüger et al. 2016] to the case of dynamical systems for finite strain thermoviscoelasticity. The application of dynamical systems in the context of viscoplasticity is proposed in [Noels et al. 2006; 2008], where variational update formulations are considered.

Our goal is the application of higher-order time-integration schemes (at least second-order accurate) so that all quantities — displacements, velocities, temperatures, and internal variables — reach second order. Commonly, first-order accurate methods are used. Even the Newmark-method has only a maximum order of two in the context of dynamical systems [Newmark 1959; Hughes 1987; Zienkiewicz and Taylor 2000]. However, it is common to treat the evolution equations on Gauss-point level with a first-order method so that the entire system cannot reach the expected order (regarding the relation of the Newmark-method in the context of Nyström-methods, see [Fritzen 1997]). Since we have a coupled system of second-order and first-order ODEs, the question arises as to what the appropriate method might be, since there are methods to treat second-order ODEs directly or the second-order ODEs are transferred into a system of first-order ODEs. Thus, two methods are considered here: first, we convert the second-order ODEs to a first-order ODE system and apply diagonally implicit Runge–Kutta (DIRK) methods to the entire system (for details concerning DIRK methods, see [Hairer et al. 1989; 1993; Hairer and Wanner 1996]). These methods have been successfully applied in the context of finite elements for isothermal and quasistatic problems in [Ellsiepen and Hartmann 2001; Hartmann 2002; Hartmann et al. 2008a] and quasistatic coupled problems in [Birken et al. 2010; Hartmann and Rothe 2013; Rothe et al. 2015b]. In the present article, the quasistatic problems are recapped as well, where a DAE system has to be solved. One intention is to show the underlying difference in the equations.

For problems in the field of linear structural dynamics, the generalized- $\alpha$  method formulated as a one-step method was originally introduced in [Chung and Hulbert 1993]. For first-order ODEs the method was introduced in [Jansen et al. 2000]. These methods show second-order accuracy in most numerical experiments, minimal numerical dissipation of lower modes, and maximal numerical dissipation of higher modes in the linear structural dynamics regime, where this numerical dissipation mechanism can be controlled by certain parameters. For first-order ODEs, an analysis of the generalized- $\alpha$  scheme was performed in [Dettmer and Perić 2003]. For the corresponding consistency and stability analysis of the generalized- $\alpha$  method for the second-order ODE system in structural dynamics, the reader is referred to [Chung and Hulbert 1993; Erlicher et al. 2002]. Furthermore, the generalized- $\alpha$  method includes the most popular classical numerical dissipative and nondissipative time integration schemes (the Newmark-family [Newmark 1959], the HHT- $\alpha$  method [Hilber et al. 1977] and the WBZ- $\alpha$  method [Wood et al.

1980]) in the field of structural dynamics. For this reason, it is a widely applied time integration scheme which has been successfully applied, for example, in [Hartmann 2007; Popp 2012; Kuhl 1996; Kuhl and Crisfield 1999; Kuhl and Ramm 1999]. Rang [2013a] proposed a simple adaptive time-step control for the one-step versions of the generalized- $\alpha$  method. A coupling between the generalized- $\alpha$  method for first-order ODEs and for second-order ODEs is presented in [Rang 2013b].

This paper is structured as follows: first, the basic equations are summarized; starting with a model problem of thermoviscoplasticity, the weak forms and their spatial discretization. Second, the time discretization is explained using DIRK and a modified generalized- $\alpha$  method. Finally, we investigate the order and efficiency of these methods by drawing on some examples.

The notation in use is defined in the following manner: geometrical vectors are symbolized by  $\vec{a}$  and second-order tensors  $\mathbf{A}$  by boldface Roman letters. We introduce matrices at the global level symbolized by boldface italic sans-serif letters  $\mathbf{A}$  and matrices on local level using the upright counterpart,  $\mathbf{A}$ .

## 2. Basic equations

In the following, the basic equations are summarized, which are: the constitutive model under consideration; the weak forms of the balance of linear momentum; the unsteady, nonlinear heat equation; and the result of the spatial discretization using finite elements.

**2.1. Constitutive model.** In the scope of our application in thermoviscoplasticity, we restrict ourselves to the case of small strains (large strains are straight forward and are embedded in the numerical schemes as well). Let  $\mathbf{E}(\vec{x}, t) = \frac{1}{2}(\text{grad } \vec{u}(\vec{x}, t) + \text{grad}^T \vec{u}(\vec{x}, t))$  be the linearized strain tensor,  $\vec{u}(\vec{x}, t)$  the displacement vector,  $\vec{x}$  the material point and  $t$  the time. Most phenomenological constitutive models are expressed by

$$\mathbf{T} = \mathbf{h}(\mathbf{E}, \Theta, \mathbf{q}), \quad (1)$$

$$\dot{\mathbf{q}}(t) = \mathbf{r}_{\mathbf{q}}(\mathbf{E}, \Theta, \mathbf{q}), \quad (2)$$

where  $\mathbf{q} \in \mathbb{R}^{n_{\mathbf{q}}}$  is the vector of internal variables,  $\mathbf{T}(\vec{x}, t)$  is the stress tensor and  $\Theta(\vec{x}, t)$  is the absolute temperature. In Table 1,  $\mathbf{q}^T = \{\mathbf{E}_v^T \mathbf{E}_r^T\}$  is given by two different strain-like internal variables in Voigt-notation, i.e.,  $n_{\mathbf{q}} = 12$ ,  $\mathbf{E}_r \in \mathbb{R}^6$ ,  $\mathbf{E}_v \in \mathbb{R}^6$ . For details of the model, see [Tsakmakis and Willuweit 2004; Rothe et al. 2015a]. Pure (thermo)elasticity is embedded as well ( $\mathbf{q} = \dot{\mathbf{q}} = \mathbf{0}$ ).

**2.2. Spatial discretization.** We investigate the partial differential equations

$$\text{div } \mathbf{T}(\vec{x}, t) + \rho(\vec{x}) \vec{k} = \rho(\vec{x}) \ddot{\vec{u}}(\vec{x}, t), \quad (3)$$

$$\hat{c}_p(\mathbf{E}, \Theta) \dot{\Theta} = \frac{1}{\rho} \text{div}(\kappa(\Theta) \text{grad } \Theta) + \hat{p}(\mathbf{E}, \dot{\mathbf{E}}, \Theta, \mathbf{E}_v, \mathbf{E}_r), \quad (4)$$

where  $\rho$  is the density,  $\vec{k}$  is the acceleration of gravity,

$$c_p = \hat{c}_p(\mathbf{E}, \Theta) = \left( c_{\Theta} - \frac{9K\alpha_{\Theta}^2}{\rho} - \frac{3c_K\alpha_{\Theta}}{\rho} \gamma(\mathbf{E}, \Theta) \right) \Theta \quad (5)$$

is the temperature- and strain-dependent heat capacity (with the abbreviation  $\gamma(\mathbf{E}, \Theta) = \mathbf{I} \cdot \mathbf{E} - 3\alpha_{\Theta}\Theta$ ),

$$\begin{aligned}
&\text{yield function: } f(\mathbf{T}, \mathbf{X}, \Theta) = \sqrt{\frac{3}{2}}(\mathbf{T} - \mathbf{X})^D \cdot (\mathbf{T} - \mathbf{X})^D - \hat{k}(\Theta) \\
&\text{elasticity relation: } \mathbf{T} = K(\Theta)(\text{tr } \mathbf{E})\mathbf{I} + 2G(\Theta)(\mathbf{E} - \mathbf{E}_v)^D - 3K(\Theta)\alpha_\Theta \vartheta \mathbf{I} \\
&\text{loading condition: } \begin{cases} \text{elasticity} & f < 0 \\ \text{viscoplasticity} & f \geq 0 \end{cases} \\
&\text{flow rules: } \begin{cases} \text{elasticity} & \dot{\mathbf{E}}_v = \mathbf{0}, \dot{\mathbf{E}}_r = \mathbf{0} \\ \text{viscoplasticity} & \dot{\mathbf{E}}_v = \lambda \frac{(\mathbf{T} - \mathbf{X})^D}{\|(\mathbf{T} - \mathbf{X})^D\|}, \dot{\mathbf{E}}_r = \lambda \beta \mathbf{X}^D \end{cases} \\
&\text{abbreviations: } \mathbf{X} = c_X \mathbf{E}_k^D = c_X (\mathbf{E}_v - \mathbf{E}_r)^D, \\
&\quad \lambda = 1/\eta \langle \hat{f}(\mathbf{T}, \mathbf{X}, \Theta) / \sigma_0 \rangle^m, \\
&\quad \hat{k}(\Theta) = (k_0 - k_H) e^{-b(\Theta - \Theta_0)} + k_H, \\
&\quad K(\Theta) = K_0 - c_K (\Theta - \Theta_0), \\
&\quad G(\Theta) = G_0 - c_G (\Theta - \Theta_0)
\end{aligned}$$

**Table 1.** Summary of constitutive equations (thermoviscoplasticity small strains).

and the heat production term due to dissipation and thermoelastic coupling is

$$p = \hat{p}(\mathbf{E}, \dot{\mathbf{E}}, \Theta, \mathbf{E}_v, \mathbf{E}_r) = \delta - \frac{\Theta}{\rho} ((3K\alpha_\Theta + c_K\gamma)\mathbf{I} + 2c_G(\mathbf{E} - \mathbf{E}_v)^D) \cdot \dot{\mathbf{E}} + \frac{\Theta}{\rho} 2c_G(\mathbf{E} - \mathbf{E}_v)^D \cdot \dot{\mathbf{E}}_v \quad (6)$$

with

$$\delta = \frac{1}{\rho\eta} \left\langle \frac{\hat{f}(\mathbf{E}, \Theta, \mathbf{E}_v, \mathbf{E}_r)}{\sigma_0} \right\rangle^m (\|2G(\Theta)(\mathbf{E} - \mathbf{E}_v)^D - c_X(\mathbf{E}_v - \mathbf{E}_r)^D\| - \beta c_X^2 \|(\mathbf{E}_v - \mathbf{E}_r)^D\|^2). \quad (7)$$

The angle brackets define Macauley brackets symbolizing a case distinction:  $\langle x \rangle = 0$  if  $x < 0$  and  $\langle x \rangle = x$  if  $x \geq 0$ . Equation (3) represents the balance of linear momentum. In view of the balance of energy (5), Fourier's model ( $\vec{q} = -\kappa(\Theta) \text{grad } \Theta$ ) is assumed, where  $\vec{q}$  defines the heat flux vector.

The partial differential equation (3) is multiplied with virtual displacements  $\delta \vec{u}(\vec{x})$  and is integrated over the volume  $V$ . The divergence theorem is applied, which leads to d'Alembert's principle

$$\int_V \underbrace{\mathbf{h}(\mathbf{E}, \Theta, \mathbf{q})}_{\mathbf{T}} \cdot \delta \mathbf{E} \, dV + \int_V \rho \ddot{\vec{u}} \cdot \delta \vec{u} \, dV = \int_A \vec{t} \cdot \delta \vec{u} \, dA + \int_V \rho \vec{k} \cdot \delta \vec{u} \, dV, \quad (8)$$

where  $\delta \mathbf{E}(\vec{x}) = (\text{grad } \delta \vec{u}(\vec{x}) + \text{grad}^T \delta \vec{u}(\vec{x}))/2$  defines the virtual strain tensor. In this context  $\delta \vec{u}(\vec{x}) = \vec{0}$  has to hold on the boundary  $A^u$  of the material body, where the displacements are prescribed;  $A = A^\sigma \cup A^u$ ;  $\vec{u}(\vec{x}, t) = \vec{\bar{u}}(t)$  on  $A^u$  (Dirichlet boundary conditions). Here,  $\vec{t}(\vec{x}, t) = \mathbf{T}(\vec{x}, t) \vec{n}(\vec{x}, t)$  defines the stress vector on the surface  $A^\sigma$ , where  $\vec{n}$  represents the surface normal and  $\vec{t}(\vec{x}, t) = \vec{\bar{t}}(\vec{x}, t)$  on  $A^\sigma$  defines the Neumann boundary conditions.

We multiply the unsteady, nonlinear heat equation (4) with the virtual temperature  $\delta \Theta$  in a similar manner, and perform both the integration over the volume as well as the application of the divergence

theorem, yielding the principle of virtual temperatures

$$\int_V \rho \hat{c}_p(\mathbf{E}, \Theta) \dot{\Theta} \delta \Theta \, dV = \int_A q \delta \Theta \, dA - \int_V \kappa(\Theta) \operatorname{grad} \Theta \cdot \operatorname{grad} \delta \Theta \, dV + \int_V \rho \hat{p}(\mathbf{E}, \dot{\mathbf{E}}, \Theta, \mathbf{q}) \delta \Theta \, dV. \quad (9)$$

The boundary conditions are:  $\Theta(\vec{x}, t) = \bar{\Theta}(\vec{x}, t)$  on the surface,  $A^\Theta$  and  $q(\vec{x}, t) = \bar{q}(\vec{x}, t)$  on  $A^q$ . Here, we assume  $q = -\bar{q} \cdot \vec{n}$  with the normal vector  $\vec{n}$  on the outer surface. Of course, mixed boundary conditions for temperature-dependent heat fluxes such as convection or radiation must be considered as well,  $q = \hat{q}(\Theta)$ . Here, we refer to [Quint et al. 2011] and the literature cited therein. The entire mathematical model considers the heat production due to mechanical dissipation in an exact manner.

In order to solve the initial boundary-value problem (3) and (4) together with constitutive models of type (1) and (2), we draw on the method of vertical lines. First, the spatial discretization is performed, followed by the time-discretization. The spatial discretization is carried out using the finite element method, i.e., an ansatz for the displacements, virtual displacements, absolute temperatures and virtual temperatures are inserted into the weak forms (8) and (9). As summarized in more detail in Appendix A, this leads to the mixed first and second-order ODE system

$$\begin{aligned} \mathbf{M}\ddot{\mathbf{u}}(t) &= -\mathbf{g}_u(t, \mathbf{u}, \Theta, \mathbf{q}) - \mathbf{M}_{\text{up}}\ddot{\bar{\mathbf{u}}}(t), \\ \mathbf{C}_\Theta(t, \mathbf{u}, \Theta)\dot{\Theta}(t) &= \mathbf{r}_\Theta(t, \mathbf{u}, \dot{\mathbf{u}}, \Theta, \mathbf{q}), \\ \dot{\mathbf{q}}(t) &= \mathbf{r}_Q(t, \mathbf{u}, \Theta, \mathbf{q}), \end{aligned} \quad (10)$$

with the initial conditions

$$\mathbf{u}(0) = \mathbf{u}_0, \quad \dot{\mathbf{u}}(0) = \mathbf{v}_0, \quad \Theta(0) = \Theta_0, \quad \mathbf{q}(0) = \mathbf{q}_0. \quad (11)$$

Equation (10)<sub>1</sub> represents the (semidiscrete) equation of motion with a constant and consistent mass matrix  $\mathbf{M} \in \mathbb{R}^{n_{\text{uu}} \times n_{\text{uu}}}$  (see (76)) which is assigned to the unknown displacement degrees of freedom (DOF)  $\mathbf{u} \in \mathbb{R}^{n_{\text{uu}}}$ . Here,  $\mathbf{M}_{\text{up}} \in \mathbb{R}^{n_{\text{uu}} \times n_{\text{up}}}$  symbolizes the mass matrix assigned to the known (prescribed) displacement DOF  $\bar{\mathbf{u}} \in \mathbb{R}^{n_{\text{up}}}$ . Thus,  $\ddot{\bar{\mathbf{u}}}(t) \in \mathbb{R}^{n_{\text{up}}}$  are the prescribed nodal accelerations, which are explicit functions of time  $t$ . The matrix  $\mathbf{C}_\Theta(t, \mathbf{u}, \Theta) \in \mathbb{R}^{n_{\Theta u} \times n_{\Theta u}}$  defines the deformation and temperature-dependent heat-capacity matrix (see (82)) where  $\Theta \in \mathbb{R}^{n_{\Theta u}}$  are the unknown nodal temperatures. The ODE system (10)<sub>3</sub> is the result of assembling all evolution equations of the internal variables into a large vector  $\mathbf{q} \in \mathbb{R}^{n_Q}$ , see the discussion in [Ellsiepen and Hartmann 2001; Hartmann 2005].

**2.2.1. Subproblems.** There are a number of subproblems which are connected to the dynamical system (10) if particular quantities do not appear, i.e., if they are neglected. In the case of  $\dot{\mathbf{q}}(t) = \mathbf{q}(t) = \mathbf{0}$ , the case of thermoelasticity under dynamical agencies is given, see (12) of Table 2. Additionally, if  $\Theta_a$  is constant spatially and temporally (where  $\Theta_a \in \mathbb{R}^{n_{\Theta a}}$ ), and  $n_{\Theta a} = n_{\Theta u} + n_{\Theta p}$  defines all nodal temperatures, pure elasto-dynamic has to be solved (see (13)). Of course, further subproblems can appear, such as:  $\mathbf{C}_\Theta = \text{constant}$  or  $\mathbf{g}_u(t, \mathbf{u}, \Theta)$  represents a linear function in  $\mathbf{u}$  and  $\Theta$ , or one-sided coupling is assumed, etc. This can be solved with specific numerical methods.

The quasistatic case holds for  $\ddot{\mathbf{u}}(t) \approx \mathbf{0}$  leading to DAE systems, see the case of thermoinelasticity (14), isothermal inelasticity (viscoelasticity, viscoplasticity) (15), and pure elasticity (16). The case of rate-independent elasto-plasticity with a yield function leads to the evolution equations  $\mathbf{A}\dot{\mathbf{q}}(t) = \mathbf{r}_Q(t, \mathbf{u}, \Theta, \mathbf{q})$ ,

$$\begin{aligned} \text{thermoelasticity: } \quad & M\ddot{\mathbf{u}}(t) = -\mathbf{g}_u(t, \mathbf{u}, \Theta) - M_{\text{up}}\ddot{\mathbf{u}}(t) \\ & \mathbf{C}_\Theta(t, \mathbf{u}, \Theta)\dot{\Theta}(t) = \mathbf{r}_\Theta(t, \mathbf{u}, \dot{\mathbf{u}}, \Theta) \end{aligned} \quad (12)$$

$$\text{elasto-dynamics: } M\ddot{\mathbf{u}}(t) = -\mathbf{g}_u(t, \mathbf{u}) - M_{\text{up}}\ddot{\mathbf{u}}(t) \quad (13)$$

$$\begin{aligned} \text{quasistatic thermoinelasticity: } \quad & \mathbf{0} = \mathbf{g}_u(t, \mathbf{u}, \Theta, \mathbf{q}) \\ & \mathbf{C}_\Theta(t, \mathbf{u}, \Theta)\dot{\Theta}(t) = \mathbf{r}_\Theta(t, \mathbf{u}, \dot{\mathbf{u}}, \Theta, \mathbf{q}) \\ & \dot{\mathbf{q}}(t) = \mathbf{r}_Q(t, \mathbf{u}, \Theta, \mathbf{q}) \end{aligned} \quad (14)$$

$$\begin{aligned} \text{quasistatic inelasticity: } \quad & \mathbf{0} = \mathbf{g}_u(t, \mathbf{u}, \mathbf{q}) \\ & \dot{\mathbf{q}}(t) = \mathbf{r}_Q(t, \mathbf{u}, \mathbf{q}) \end{aligned} \quad (15)$$

$$\text{elasticity: } \mathbf{0} = \mathbf{g}_u(t, \mathbf{u}) \quad (16)$$

**Table 2.** Dynamical and quasistatic subproblems.

where  $\mathbf{A}$  is a singular matrix and  $\mathbf{r}$  contains case distinctions (see the discussion in [Ellsiepen and Hartmann 2001]).

**2.2.2. Reaction force computation.** Another question connected to the dynamical systems under consideration is related to the computation of the reaction forces at those degrees of freedom, where the displacements are prescribed. This is not provided by d'Alembert's principle (8) since the virtual displacements vanish at those DOF for which the displacements are prescribed (and no virtual work is produced). The same situation holds for the heat flux computation for those nodes with prescribed temperatures.

This is consistently discussed for isothermal quasistatic problems in [Hartmann 2005] and the literature cited therein. Hamkar [2013] treats this issue for quasistatic thermomechanical problems since other time-integration methods require these investigations. He applies a concept developed by Gear [1986]. The basic idea is as follows: we assume that all displacement DOF  $\mathbf{u}_a \in \mathbb{R}^{n_{\text{uu}}+n_{\text{up}}}$  are unknown. The vector is decomposed into DOF that are connected to Dirichlet boundary conditions and the remaining quantities,

$$\mathbf{u}_a(t) = \begin{cases} \mathbf{u}(t) \\ \hat{\mathbf{u}}(t) \end{cases} \quad \text{with } \mathbf{u} \in \mathbb{R}^{n_{\text{uu}}} \text{ and } \hat{\mathbf{u}} \in \mathbb{R}^{n_{\text{up}}}.$$

Consistently, all virtual displacements are arbitrary,  $\delta\mathbf{u}_a \in \mathbb{R}^{n_{\text{uu}}+n_{\text{up}}}$ . However, there is the constraint equation

$$\mathbf{c}_u(t, \mathbf{a}_a) = \mathbf{Z}_u^T \mathbf{u}_a(t) - \bar{\mathbf{u}}(t) = \hat{\mathbf{u}}(t) - \bar{\mathbf{u}}(t) = \mathbf{0} \quad (17)$$

at the DOF for which displacements are prescribed, with

$$\mathbf{Z}_u = \begin{bmatrix} \mathbf{0}_{n_{\text{uu}} \times n_{\text{up}}} \\ \mathbf{I}_{n_{\text{up}} \times n_{\text{up}}} \end{bmatrix}, \quad \mathbf{Z}_u \in \mathbb{R}^{(n_{\text{uu}}+n_{\text{up}}) \times n_{\text{up}}}$$

and the prescribed functions  $\bar{\mathbf{u}}(t) \in \mathbb{R}^{n_{\text{up}}}$ . Additionally, the weak form changes to

$$\delta \mathbf{u}_a^T \{ \mathbf{M}_a \ddot{\mathbf{u}}_a(t) + \mathbf{g}_{\text{ua}}(t, \mathbf{u}_a, \boldsymbol{\Theta}_a, \mathbf{q}) - \mathbf{Z}_u \lambda_u(t) \} = 0,$$

i.e., there is an additional term defined by the Lagrange-multiplier  $\lambda_u \in \mathbb{R}^{n_{\text{up}}}$ . In other words,

$$\begin{aligned} & \mathbf{M}_a \ddot{\mathbf{u}}_a(t) + \mathbf{g}_{\text{ua}}(t, \mathbf{u}_a, \boldsymbol{\Theta}_a, \mathbf{q}) - \mathbf{Z}_u \lambda_u(t) \\ &= \begin{bmatrix} \mathbf{M} & \mathbf{M}_{\text{up}} \\ \mathbf{M}_{\text{pu}} & \mathbf{M}_{\text{pu}} \end{bmatrix} \begin{Bmatrix} \ddot{\mathbf{u}}(t) \\ \ddot{\hat{\mathbf{u}}}(t) \end{Bmatrix} + \begin{Bmatrix} \mathbf{g}_u(t, \mathbf{u}, \hat{\mathbf{u}}, \boldsymbol{\Theta}, \hat{\boldsymbol{\Theta}}, \mathbf{q}) \\ \hat{\mathbf{g}}_u(t, \mathbf{u}, \hat{\mathbf{u}}, \boldsymbol{\Theta}, \hat{\boldsymbol{\Theta}}, \mathbf{q}) - \lambda_u(t) \end{Bmatrix} = \mathbf{0} \end{aligned} \quad (18)$$

has to be solved in combination with the constraint (17). The same idea holds for the heat equation having the constraint

$$\mathbf{c}_{\Theta}(t, \boldsymbol{\Theta}_a) = \mathbf{Z}_{\Theta}^T \boldsymbol{\Theta}_a(t) - \bar{\boldsymbol{\Theta}}(t) = \hat{\boldsymbol{\Theta}}(t) - \bar{\boldsymbol{\Theta}}(t) = \mathbf{0} \quad (19)$$

for the given nodal temperature functions  $\bar{\boldsymbol{\Theta}}(t) \in \mathbb{R}^{n_{\Theta \text{p}}}$ . The modified weak form reads

$$\delta \boldsymbol{\Theta}_a^T \{ \mathbf{C}_{\Theta a}(t, \mathbf{u}_a, \boldsymbol{\Theta}_a) \dot{\boldsymbol{\Theta}}_a(t) - \mathbf{r}_{\Theta a}(t, \mathbf{u}_a, \dot{\mathbf{u}}_a, \boldsymbol{\Theta}_a, \mathbf{q}) - \mathbf{Z}_{\Theta} \lambda_{\Theta}(t) \} = 0,$$

with the Lagrange multiplier  $\lambda_{\Theta}(t) \in \mathbb{R}^{n_{\Theta \text{p}}}$  and the matrix

$$\mathbf{Z}_{\Theta} = \begin{bmatrix} \mathbf{0}_{n_{\Theta \text{u}} \times n_{\Theta \text{p}}} \\ \mathbf{I}_{n_{\Theta \text{p}} \times n_{\Theta \text{p}}} \end{bmatrix}, \mathbf{Z}_{\Theta} \in \mathbb{R}^{(n_{\Theta \text{u}} + n_{\Theta \text{p}}) \times n_{\Theta \text{p}}}.$$

The decomposition yields the ODE system

$$\begin{bmatrix} \mathbf{C}_{\Theta} & \mathbf{C}_{\Theta \text{up}} \\ \mathbf{C}_{\Theta \text{pu}} & \mathbf{C}_{\Theta \text{pp}} \end{bmatrix} \begin{Bmatrix} \dot{\boldsymbol{\Theta}}(t) \\ \dot{\hat{\boldsymbol{\Theta}}}(t) \end{Bmatrix} = \begin{Bmatrix} \mathbf{r}_{\Theta}(t, \mathbf{u}, \hat{\mathbf{u}}, \dot{\mathbf{u}}, \dot{\hat{\mathbf{u}}}, \boldsymbol{\Theta}, \hat{\boldsymbol{\Theta}}, \mathbf{q}) \\ \hat{\mathbf{r}}_{\Theta}(t, \mathbf{u}, \hat{\mathbf{u}}, \dot{\mathbf{u}}, \dot{\hat{\mathbf{u}}}, \boldsymbol{\Theta}, \hat{\boldsymbol{\Theta}}, \mathbf{q}) + \lambda_{\Theta}(t) \end{Bmatrix}. \quad (20)$$

Table 3 summarizes the entire DAE system. For the case of quasistatic and isothermal problems and implicit finite elements, see [Hartmann et al. 2008b].

### 3. Time discretization schemes

In the following we propose two implicit time integration methods to treat the ODE system (10) since we are interested in a low frequency response. Explicit methods are widely used in the context of high frequency responses and wave-like phenomena—or in high velocity impact situations, where contact

$$\begin{aligned} & \mathbf{M}_a \ddot{\mathbf{u}}_a(t) = -\mathbf{g}_{\text{ua}}(t, \mathbf{u}_a, \boldsymbol{\Theta}_a, \mathbf{q}) + \mathbf{Z}_u \lambda_u(t) \\ & \mathbf{Z}_u^T \mathbf{u}_a(t) - \bar{\mathbf{u}}(t) = \mathbf{0} \\ & \mathbf{C}_{\Theta a}(t, \mathbf{c} \mathbf{r}_a, \boldsymbol{\Theta}_a) \dot{\boldsymbol{\Theta}}_a(t) = \mathbf{r}_{\Theta a}(t, \mathbf{u}_a, \dot{\mathbf{u}}_a, \boldsymbol{\Theta}_a, \mathbf{q}) + \mathbf{Z}_{\Theta} \lambda_{\Theta}(t) \\ & \mathbf{Z}_{\Theta}^T \boldsymbol{\Theta}_a(t) - \bar{\boldsymbol{\Theta}}(t) = \mathbf{0} \\ & \dot{\mathbf{q}}(t) = \mathbf{r}_Q(\mathbf{u}_a, \boldsymbol{\Theta}_a, \mathbf{q}) \end{aligned} \quad (21)$$

**Table 3.** Entire DAE system if reaction force and reaction heat flux have to be determined



conditions dominate the problem. Implicit methods have the advantage in that it is possible to apply relatively large time-step sizes in comparison to explicit schemes. However, the implementation of implicit methods is more challenging due to the fact that nonlinear solution methods have to be considered, see in this context [Belytschko et al. 2000].

Since we are interested in one-step methods, we follow the numerical schemes in [Ellsiepen and Hartmann 2001] (see [Fritzen 1997] for problems concerning the aspect of dynamics). Accordingly, the ODE part of second order is transferred into a system of first-order ODEs and stiffly accurate diagonally implicit Runge–Kutta methods are applied. A second method is an extension of the generalized- $\alpha$  method seen in [Chung and Hulbert 1993]. Here, we draw on a one-step formulation.

In contrast to these methods, there are multistep methods that require a special starting procedure as well as access to time-step information reaching back even further than  $t_n$ .

**3.1. DIRK methods.** In order to obtain a basic background of the proposed time integration scheme, we recall the general class of implicit Runge–Kutta methods (IRK) applied to (10) [Strehmel et al. 2012; Hairer et al. 1993]. In the next step, we introduce the class of diagonally implicit Runge–Kutta (DIRK) methods using a special choice of algorithmic parameters in order to obtain the important goal of computational efficiency. To this end, we transform the coupled system of second-order ODEs in (10) to a first-order ODE system by exploiting the trivial equation  $\dot{\mathbf{u}} = \mathbf{v}(t)$ . Accordingly, the system

$$\begin{aligned} M\dot{\mathbf{v}}(t) &= -\mathbf{g}_u(t, \mathbf{u}, \Theta, \mathbf{q}) - M_{\text{up}}\dot{\hat{\mathbf{v}}}(t), \\ \dot{\mathbf{u}}(t) &= \mathbf{v}(t), \\ \mathbf{C}_\Theta(t, \mathbf{u}, \Theta)\dot{\Theta}(t) &= \mathbf{r}_\Theta(t, \mathbf{u}, \mathbf{v}, \Theta, \mathbf{q}), \\ \dot{\mathbf{q}}(t) &= \mathbf{r}_Q(t, \mathbf{u}, \Theta, \mathbf{q}), \end{aligned} \tag{22}$$

must be solved. To achieve a high-order method, we divide the integration step from time  $t_n$  to  $t_{n+1}$  in further points in time

$$T_{ni} = t_n + c_i \Delta t_n, \quad i = 1, \dots, s, \tag{23}$$

with coefficients  $c_i$ ,  $i = 1, \dots, s$ . These points are called *stages*, where  $s$  defines the number of stages. At every stage, the stage variables in the corresponding field are defined according to

$$\begin{aligned} \mathbf{U}_{ni} &= \mathbf{u}_n + \Delta t_n \sum_{j=1}^s a_{ij} \mathbf{V}_{nj}, & \mathbf{V}_{ni} &= \mathbf{v}_n + \Delta t_n \sum_{j=1}^s a_{ij} \mathbf{A}_{nj}, \\ \Theta_{ni} &= \Theta_n + \Delta t_n \sum_{j=1}^s a_{ij} \dot{\Theta}_{nj}, & \mathbf{Q}_{ni} &= \mathbf{q}_n + \Delta t_n \sum_{j=1}^s a_{ij} \dot{\mathbf{Q}}_{nj}, \end{aligned} \tag{24}$$

with weighting factors  $a_{ij}$ . The index  $ni$  denotes the  $i$ -th stage at time  $T_{ni}$ . Formally, we now have two sets of unknowns, namely the so-called *stage values*  $\mathbf{U}_{ni}$ ,  $\mathbf{V}_{ni}$ ,  $\Theta_{ni}$ ,  $\mathbf{Q}_{ni}$  (displacements, velocities, temperatures and internal variables) and the *stage derivatives*  $\mathbf{V}_{ni}$ ,  $\mathbf{A}_{ni}$ ,  $\dot{\Theta}_{ni}$ ,  $\dot{\mathbf{Q}}_{ni}$ . However, since they are not independent, due to (24), we choose the stage derivatives  $\mathbf{V}_{ni}$ ,  $\mathbf{A}_{ni}$ ,  $\dot{\Theta}_{ni}$  for the following explanations, and the stage value  $\mathbf{Q}_{ni}$  as the primary unknown for the internal variables. Since we are looking for the approximate solution at  $t_{n+1}$ , we need a relation which maps the stage derivatives to the unknown

$\begin{array}{c cccc} c_1 & a_{11} & a_{12} & \cdots & a_{1s} \\ c_2 & a_{21} & a_{22} & \cdots & a_{2s} \\ \vdots & \vdots & & \ddots & \vdots \\ c_s & a_{s1} & a_{s2} & \cdots & a_{ss} \\ \hline & b_1 & b_2 & \cdots & b_s \end{array}$ <p>(a) IRK method</p>	$\begin{array}{c cccc} c_1 & a_{11} & 0 & \cdots & 0 \\ c_2 & a_{21} & a_{22} & \ddots & \vdots \\ \vdots & \vdots & & \ddots & 0 \\ c_s & b_1 & b_2 & \cdots & b_s \\ \hline & b_1 & b_2 & \cdots & b_s \end{array}$ <p>(b) SDIRK method</p>	$\begin{array}{c c} \mathbf{c} & \mathbf{A} \\ \hline & \mathbf{b}^T \end{array}$ <p>(c) RK scheme</p>	$\begin{array}{c c c} \mathbf{c} & \overline{\mathbf{A}} & \mathbf{A} \\ \hline & \overline{\mathbf{b}}^T & \mathbf{b}^T \end{array}$ <p>(d) Indirect RKN scheme</p>
---	---	--	--

**Figure 1.** Butcher-tableaus.

quantities at  $t_{n+1}$ . These integration formulas are based on quadrature rules in [Hairer et al. 1993; Hairer and Wanner 1996; Strehmel et al. 2012] and are defined by

$$\begin{aligned} \mathbf{u}_{n+1} &= \mathbf{u}_n + \Delta t_n \sum_{i=1}^s b_i \mathbf{V}_{ni}, & \mathbf{v}_{n+1} &= \mathbf{v}_n + \Delta t_n \sum_{i=1}^s b_i \mathbf{A}_{ni}, \\ \boldsymbol{\Theta}_{n+1} &= \boldsymbol{\Theta}_n + \Delta t_n \sum_{i=1}^s b_i \dot{\boldsymbol{\Theta}}_{ni}, & \mathbf{q}_{n+1} &= \mathbf{q}_n + \Delta t_n \sum_{i=1}^s b_i \dot{\mathbf{Q}}_{ni}, \end{aligned} \quad (25)$$

with the weighting factors  $b_i$ ,  $i = 1, \dots, s$ . The weighting factors  $a_{ij}$ ,  $b_i$ , and  $c_i$  are usually summarized in a Butcher array to distinguish different classes of Runge–Kutta methods, see Figure 1(a). These factors are defined and calculated in order to obtain efficient, stable and accurate methods. By applying the general implicit Runge–Kutta scheme to (22) (i.e., inserting the primary variables and the relations of (24)), we obtain (for  $i = 1, \dots, s$ )

$$\begin{aligned} \mathbf{M} \mathbf{A}_{ni} &= -\mathbf{g}_u(T_{ni}, \mathbf{U}_{ni}(\mathbf{A}_{nj}), \boldsymbol{\Theta}_{ni}(\dot{\boldsymbol{\Theta}}_{nj}), \mathbf{Q}_{ni}) - \mathbf{M}_{\text{up}} \ddot{\mathbf{u}}(T_{ni}), \\ \mathbf{V}_{ni}(\mathbf{A}_{nj}) &= \mathbf{v}_n + \Delta t_n \sum_{j=1}^s a_{ij} \mathbf{A}_{nj}, \quad j = 1, \dots, s, \\ \mathbf{C}_{\ominus}(\mathbf{U}_{ni}, \boldsymbol{\Theta}_{ni}) \dot{\boldsymbol{\Theta}}_{ni} &= \mathbf{r}_{\ominus}(T_{ni}, \mathbf{U}_{ni}(\mathbf{A}_{nj}), \mathbf{V}_{ni}(\mathbf{A}_{nj}), \boldsymbol{\Theta}_{ni}(\dot{\boldsymbol{\Theta}}_{nj}), \mathbf{Q}_{ni}), \\ \dot{\mathbf{Q}}_{ni}(\mathbf{Q}_{nj}) &= \mathbf{r}_{\mathbf{Q}}(T_{ni}, \mathbf{U}_{ni}(\mathbf{A}_{nj}), \boldsymbol{\Theta}_{ni}(\dot{\boldsymbol{\Theta}}_{nj}), \mathbf{Q}_{ni}), \end{aligned} \quad (26)$$

a coupled nonlinear system of equations with the dimension  $(2n_{\text{uu}} + n_{\ominus u} + n_{\mathbf{Q}}) \times s$  in each time-step  $\Delta t_n$ , where all stage unknowns are coupled. Next, we can eliminate  $\mathbf{V}_{ni}$  in (25)<sub>1</sub> and (24)<sub>1</sub> by exploiting (26)<sub>2</sub>. Furthermore, we assume existing stability requirements in the form of

$$c_i = \sum_{j=1}^s a_{ij}, \quad \sum_{i=1}^s b_i = 1, \quad (27)$$

$$\begin{array}{c|cc}
0 & 0 & 0 \\
1 & \frac{1}{2} - \beta & \beta \\
\hline
& \frac{1}{2} - \beta & \beta \\
\hline
& 1 - \gamma & \gamma
\end{array}
\qquad
\begin{array}{c|c}
c & \bar{\mathbf{A}} \\
\hline
& \bar{\mathbf{b}}^T \\
\hline
& \mathbf{b}^T
\end{array}$$

**Figure 2.** Butcher tableau for Newmark-method and presentation of schematic direct RKN scheme: Newmark-methods embedded as Nyström-method (left) and Nyström-scheme (right).

which ensures a consistent method and applicability for nonautonomous ODEs. This leads to

$$\mathbf{U}_{ni} = \mathbf{u}_{n+1} + c_i \Delta t_n \mathbf{v}_n + \Delta t_n^2 \sum_{j=1}^s \bar{a}_{ij} \mathbf{A}_{nj}, \quad (28)$$

$$\mathbf{u}_{n+1} = \mathbf{u}_n + \Delta t_n \mathbf{v}_n + \Delta t_n^2 \sum_{i=1}^s \bar{b}_i \mathbf{A}_{ni}, \quad (29)$$

with the new coefficients

$$\bar{a}_{ij} = \sum_{k=1}^s a_{ik} a_{kj}, \quad \text{and} \quad \bar{b}_i = \sum_{j=1}^s b_j a_{ji}. \quad (30)$$

This approach is identical to the construction of an indirect Runge–Kutta–Nyström method (RKN) by consistent application of an underlying Runge–Kutta scheme [Hairer et al. 1993; Strehmel et al. 2012; Fritzen 1997]. A schematic Butcher-tableau for an indirect RKN method is depicted in Figure 1(d). The stage quantities  $\mathbf{U}_{ni}$  and  $\mathbf{V}_{ni}$  can now be expressed as functions of the stage acceleration  $\mathbf{A}_{nj}$ , so that it is sufficient to store only the stage derivatives. For a pure structural dynamical problem, it is possible to save half the storage.

There are further schemes apart from these indirectly constructed Runge–Kutta–Nyström methods. We call them direct Runge–Kutta–Nyström methods if the conditions in (30) do not exist and if the weighting factors  $\bar{a}_{ij}$  and  $\bar{b}_i$  are independent from  $a_{ij}$  and  $b_i$ . The direct RKN methods are principally applicable to first-order ODEs and to coupled systems, such as the one presented in (10). These methods were originally developed for general second-order ODEs. Furthermore, in the case of second-order ODEs which are not coupled with ODEs of first order and do not depend on  $\dot{\mathbf{u}}$  (i.e.,  $\mathbf{g}_u$  does not depend on  $\dot{\mathbf{u}}$ , see the case of structural dynamics in (13)), the coefficients  $a_{ij}$  are no longer needed. Methods for which no coefficient matrix  $\mathbf{A}$  is given are called *Nyström methods* [Hairer et al. 1993], see Figure 2 (right). However, taking (24)<sub>2</sub>–(24)<sub>4</sub> in to account, these coefficients are indispensable. Fritzen [1997] showed that the popular Newmark-family is included in the class of diagonally implicit, direct Runge–Kutta–Nyström (DIRKN) methods in form of the Butcher-tableau in Figure 2 (left), with the well-known algorithmic parameters  $\gamma \in [0, 1]$  and  $\beta \in [0, 1/2]$  determining the stability and accuracy behavior (see Section 3.2). Because of the restrictions regarding  $\dot{\mathbf{u}}$  mentioned above and the treatment of ODEs, portions of first-order general Newmark methods with arbitrary algorithmic parameter combinations are not applicable to (10). There exists one exception to this statement. The trapezoidal rule, which is known as the constant average acceleration method (CAA) in structural dynamics literature, is considered the most effective

if the parameters  $\{\gamma = 1/2, \beta = 1/4\}$  are chosen [Hughes 1987]. This second-order method fits into the class of DIRK methods [Ellsiepen and Hartmann 2001]. For this reason, the trapezoidal rule is the method of choice if we solve (10) with a Newmark-scheme (see [Ortiz and Popov 1985] for additional information regarding the trapezoidal rule).

The computational expense of a solution using IRK methods is high and thus is a drawback compared to other time integration methods. To decouple the stage quantities and to preserve the sparse structure of the linearized finite element system, we use DIRK methods where  $a_{ij} = 0$  and — with regard to (30)<sub>1</sub> —  $\bar{a}_{ij} = 0$  for  $j > i$  holds (compare Figures 1(a) and 1(b)). In this case, the integration step for each field variable reduces to

$$\begin{aligned} \mathbf{U}_{ni} &= \mathbf{U}_{ni}^S + \Delta t_n^2 \bar{a}_{ii} \mathbf{A}_{ni}, & \mathbf{V}_{ni} &= \mathbf{V}_{ni}^S + \Delta t_n a_{ii} \mathbf{A}_{ni}, \\ \boldsymbol{\Theta}_{ni} &= \boldsymbol{\Theta}_{ni}^S + \Delta t_n a_{ii} \dot{\boldsymbol{\Theta}}_{ni}, & \mathbf{Q}_{ni} &= \mathbf{Q}_{ni}^S + \Delta t_n a_{ii} \dot{\mathbf{Q}}_{ni}, \end{aligned} \quad (31)$$

with starting values

$$\begin{aligned} \mathbf{U}_{ni}^S &= \mathbf{u}_n + c_i \Delta t_n \mathbf{v}_n + \Delta t_n^2 \sum_{j=1}^{i-1} \bar{a}_{ij} \mathbf{A}_{nj}, & \mathbf{V}_{ni}^S &= \mathbf{v}_n + \Delta t_n \sum_{j=1}^{i-1} a_{ij} \mathbf{A}_{nj}, \\ \boldsymbol{\Theta}_{ni}^S &= \boldsymbol{\Theta}_n + \Delta t_n \sum_{j=1}^{i-1} a_{ij} \dot{\boldsymbol{\Theta}}_{nj}, & \mathbf{Q}_{ni}^S &= \mathbf{q}_n + \Delta t_n \sum_{j=1}^{i-1} a_{ij} \dot{\mathbf{Q}}_{nj}, \end{aligned} \quad (32)$$

depending only on stage derivatives already calculated in previous stages. In each time-step — due to the decoupling of the stage quantities — we have to consecutively solve a sequence of  $s$  nonlinear systems of equations with  $n_{uu} + n_{\Theta u} + n_Q$  unknowns  $(\mathbf{A}_{ni}, \dot{\boldsymbol{\Theta}}_{ni}, \mathbf{Q}_{ni})$  of the form

$$\begin{aligned} \mathbf{G}_u(T_{ni}, \mathbf{A}_{ni}, \dot{\boldsymbol{\Theta}}_{ni}, \mathbf{Q}_{ni}) &= \mathbf{M} \mathbf{A}_{ni} + \mathbf{g}_u(T_{ni}, \mathbf{U}_{ni}(\mathbf{A}_{ni}), \boldsymbol{\Theta}_{ni}(\dot{\boldsymbol{\Theta}}_{ni}), \mathbf{Q}_{ni}) + \mathbf{M}_{\text{up}} \ddot{\mathbf{u}}(T_{ni}) = \mathbf{0}, \\ \mathbf{G}_{\Theta}(T_{ni}, \mathbf{A}_{ni}, \dot{\boldsymbol{\Theta}}_{ni}, \mathbf{Q}_{ni}) &= \mathbf{C}_{\Theta}(\mathbf{U}_{ni}, \boldsymbol{\Theta}_{ni}) \dot{\boldsymbol{\Theta}}_{ni} \\ &\quad - \mathbf{r}_{\Theta}(T_{ni}, \mathbf{U}_{ni}(\mathbf{A}_{ni}), \mathbf{V}_{ni}(\mathbf{A}_{ni}), \boldsymbol{\Theta}_{ni}(\dot{\boldsymbol{\Theta}}_{ni}), \mathbf{Q}_{ni}) = \mathbf{0}, \\ \mathbf{L}(T_{ni}, \mathbf{A}_{ni}, \dot{\boldsymbol{\Theta}}_{ni}, \mathbf{Q}_{ni}) &= \mathbf{Q}_{ni} - \mathbf{Q}_{ni}^S - \Delta t_n a_{ii} \mathbf{r}_Q(T_{ni}, \mathbf{U}_{ni}(\mathbf{A}_{ni}), \boldsymbol{\Theta}_{ni}(\dot{\boldsymbol{\Theta}}_{ni}), \mathbf{Q}_{ni}) = \mathbf{0}. \end{aligned} \quad (33)$$

Equation (31)<sub>4</sub> can be rearranged to

$$\dot{\mathbf{Q}}_{ni} = \frac{\mathbf{Q}_{ni} - \mathbf{Q}_{ni}^S}{\Delta t_n a_{ii}}. \quad (34)$$

In other words, we have to solve the nonlinear system of equations

$$\begin{aligned} \mathbf{G}_u(\mathbf{A}_{ni}, \dot{\boldsymbol{\Theta}}_{ni}, \mathbf{Q}_{ni}) &= \mathbf{0}, \\ \mathbf{G}_{\Theta}(\mathbf{A}_{ni}, \dot{\boldsymbol{\Theta}}_{ni}, \mathbf{Q}_{ni}) &= \mathbf{0}, \\ \mathbf{L}(\mathbf{A}_{ni}, \dot{\boldsymbol{\Theta}}_{ni}, \mathbf{Q}_{ni}) &= \mathbf{0}, \end{aligned} \quad (35)$$

at each stage  $T_{ni}$  to obtain the stage quantities (i.e., the acceleration  $\mathbf{A}_{ni}$ , the temperature-rate  $\dot{\boldsymbol{\Theta}}_{ni}$  and the internal variables  $\mathbf{Q}_{ni}$ ). Here, we have omitted the stage time  $T_{ni}$  for brevity. This is done using the multilevel Newton algorithm (MLNA) in [Rabbat et al. 1979]; regarding finite elements, see [Ellsiepen and Hartmann 2001; Hartmann 2005].

After solving these systems, the stage derivatives are known and the final solution at time  $t_{n+1}$  is computable by the sum (29) and (25)<sub>2–(25)</sub><sub>4</sub>.

At this point we would like to remark that for DAE systems resulting from the quasistatic case, stiffly accurate methods are preferable [Ellsiepen and Hartmann 2001; Hartmann 2002; Hartmann et al. 2008a; Birken et al. 2010; Hartmann and Rothe 2013; Rothe et al. 2015b]. Here, the solution variables  $\mathbf{A}_{ns}$ ,  $\dot{\Theta}_{ns}$ ,  $\mathbf{Q}_{ns}$  in the last stage coincide with the new solution at time  $t_{n+1}$ ,  $\mathbf{a}_{n+1} = \mathbf{A}_{ns}$ ,  $\dot{\Theta}_{n+1} = \dot{\Theta}_{ns}$ ,  $\mathbf{q}_{n+1} = \mathbf{Q}_{ns}$ . This property guarantees that the algebraic constraints are fulfilled at the new time-step [Prothero and Robinson 1974]. With regard to the Butcher-tableaus in Figure 1(b), stiff accuracy implies a regular coefficient matrix  $\mathbf{A}$  satisfying  $a_{si} = b_i$  and  $\bar{a}_{si} = \bar{b}_i$ . From (24) and (25) it is obvious that this results in the mentioned equivalence. Thus, the latter equation can be omitted, saving additional computational time. In Section 4, we draw on stiffly accurate, diagonally implicit Runge–Kutta (SDIRK) methods for our numerical examples in order to treat the quasistatic as well as the dynamic case.

**3.2. Generalized- $\alpha$  method.** In this section we apply the generalized- $\alpha$  method, formulated as a one-step method, which was originally introduced in [Chung and Hulbert 1993] for second-order ODEs in the field of computational solid dynamics. This unconditionally stable method allows us to introduce controllable numerical dissipation into the considered system. For a special choice of the integration parameter set consisting of the algorithmic parameters  $\alpha_f$ ,  $\alpha_m$ ,  $\beta$  and  $\gamma$ , the generalized- $\alpha$  method includes the most popular classical numerical dissipative and nondissipative time integration schemes (for more details regarding the Newmark-family [Newmark 1959], the HHT- $\alpha$  method [Hilber et al. 1977] and the WBZ- $\alpha$  method [Wood et al. 1980], see [Kuhl and Crisfield 1999]). In many publications [Chung and Hulbert 1993; Jansen et al. 2000; Erlicher et al. 2002; Popp 2012], the proposed single-step version of the integrator, which comprises a special parameter set, is assumed to be second-order accurate at all times. In [Rang 2013a; 2013b], however, it was shown that this statement holds only for a particular parameter set, which is not identical to the commonly used one, since there is a distinction between the one-step and the multistep version [Erlicher et al. 2002]. These parameter sets  $\{\alpha_f, \alpha_m, \beta, \gamma\}$  are often expressed in terms of a spectral radius  $\rho_\infty \in [0, 1]$  as the sole free parameter

$$\alpha_f = \frac{1}{1 + \rho_\infty}, \quad \alpha_m = \frac{2 - \rho_\infty}{1 + \rho_\infty}, \quad \gamma = \frac{1}{2} + \alpha_m - \alpha_f, \quad \beta = \frac{1}{4}(1 + \alpha_m - \alpha_f)^2. \quad (36)$$

The given setting follows directly from requirements of unconditional stability, optimized numerical dissipation, and second-order accuracy for the multistep method. The spectral radius  $\rho_\infty$  controls the high-frequency dissipation, whereas  $\rho_\infty = 1$  designates the no dissipation case, and  $\rho_\infty = 0$  means full annihilation [Chung and Hulbert 1993; Kuhl and Crisfield 1999; Jansen et al. 2000; Popp 2012]. Furthermore,  $\rho_\infty$  ensures algorithmic parameters leading to optimal time integration schemes. In the linear structural dynamic regime, this leads to maximized high-frequency dissipation, while damping for the important lower modes is kept at a minimum. However, if these parameter sets are used for the one-step method, it is theoretically only possible to reach first order. The error constant in this case is very small, so the observed numerical order of convergence is two. Moreover, in [Rang 2013b], the one-step version of the generalized- $\alpha$  method applied to second and first-order ODEs obtains better results than the corresponding multistep version.

The chosen notation in this paper for the generalized- $\alpha$  method is based on the works of Rang [2013a; 2013b] and Jansen et al. [2000]. In the following, we apply the one-step version of the generalized- $\alpha$

method for second-order ODEs to the semidiscrete equations of motion (10)<sub>1</sub> and use the presented algorithmic parameter set  $\{\alpha_f, \alpha_m, \beta, \gamma\}$  as a function of  $\rho_\infty$ . We start with linear interpolation rules for the generalized mid-point quantities which are commonly established for the generalized- $\alpha$  method,

$$\mathbf{U}_{n+\alpha_f} = \alpha_f \mathbf{u}_{n+1} + (1-\alpha_f) \mathbf{u}_n, \quad \dot{\mathbf{U}}_{n+\alpha_f} = \alpha_f \mathbf{v}_{n+1} + (1-\alpha_f) \mathbf{v}_n, \quad \ddot{\mathbf{U}}_{n+\alpha_m} = \alpha_m \mathbf{a}_{n+1} + (1-\alpha_m) \mathbf{a}_n. \quad (37)$$

Now, we introduce the well-known Newmark [1959] approximations to describe the discrete velocities  $\mathbf{v}_{n+1}$  and accelerations  $\mathbf{a}_{n+1}$  at  $t_{n+1}$  as functions of the unknown displacements  $\mathbf{u}_{n+1}$  and in terms of already known quantities at time  $t_n$ ,

$$\mathbf{v}_{n+1} = \frac{\gamma}{\beta \Delta t_n} (\mathbf{u}_{n+1} - \mathbf{u}_n) - \frac{\gamma - \beta}{\beta} \mathbf{v}_n - \frac{\gamma - 2\beta}{2\beta} \Delta t_n \mathbf{a}_n, \quad (38)$$

$$\mathbf{a}_{n+1} = \frac{1}{\beta \Delta t_n^2} (\mathbf{u}_{n+1} - \mathbf{u}_n) - \frac{1}{\beta \Delta t_n} \mathbf{v}_n - \frac{1 - 2\beta}{2\beta} \mathbf{a}_n. \quad (39)$$

The generalized midpoint velocities and accelerations in (37) can be expressed as function of the displacements  $\mathbf{u}_{n+1}$ ,

$$\dot{\mathbf{U}}_{n+\alpha_f} = \frac{\alpha_f \gamma}{\beta \Delta t_n} (\mathbf{u}_{n+1} - \mathbf{u}_n) - \frac{\alpha_f \gamma - \beta}{\beta} \mathbf{v}_n - \frac{(\gamma - 2\beta) \alpha_f}{2\beta} \Delta t_n \mathbf{a}_n, \quad (40)$$

$$\ddot{\mathbf{U}}_{n+\alpha_m} = \frac{\alpha_m}{\beta \Delta t_n^2} (\mathbf{u}_{n+1} - \mathbf{u}_n) - \frac{\alpha_m}{\beta \Delta t_n} \mathbf{v}_n - \frac{\alpha_m - 2\beta}{2\beta} \mathbf{a}_n. \quad (41)$$

By applying the generalized- $\alpha$  method to the semidiscrete equation of motion (10)<sub>1</sub> with

$$T_{n+\alpha_f} = t_n + \alpha_f \Delta t_n = \alpha_f t_{n+1} + (1 - \alpha_f) t_n \quad (42)$$

and

$$T_{n+\alpha_m} = t_n + \alpha_m \Delta t_n = \alpha_m t_{n+1} + (1 - \alpha_m) t_n, \quad (43)$$

we obtain the discrete linear momentum balance, i.e., the fully (meaning in space and time) discretized finite element formulation of nonlinear structural dynamics. This modified structural equation of motion, evaluated at some instant inside  $[t_n, t_{n+1}]$ , reads

$$\mathbf{G}_u(t_{n+1}, \mathbf{u}_{n+1}, \boldsymbol{\Theta}_{n+1}, \mathbf{q}_{n+1}) = \mathbf{M} \ddot{\mathbf{U}}_{n+\alpha_m} + \mathbf{g}_u(T_{n+\alpha_f}, \mathbf{U}_{n+\alpha_f}, \boldsymbol{\Theta}_{n+\alpha_f}, \mathbf{Q}_{n+\alpha_f}) + \mathbf{M}_{\text{up}} \ddot{\mathbf{U}}(T_{n+\alpha_m}) = \mathbf{0}, \quad (44)$$

where we have to evaluate the internal forces and external forces at the midpoint  $n + \alpha_f$ , which occur in  $\mathbf{g}_u$  defined in (75). This is a midpoint-type approach. In this way we obtain an equivalent equation structure and can use the same material and element routines as for the DIRK integrators. Alternatively, a linear interpolation for  $\mathbf{g}_u$  based on a trapezoidal rule can be applied [Kuhl and Crisfield 1999; Erlicher et al. 2002; Popp 2012]. For the linear case (small deformation and linear elastic material behavior) both approaches are equivalent.

At this point, we would like to briefly mention the so-called energy-momentum conserving time integration schemes [Simo and Tarnow 1992; Simo et al. 1992; Gonzalez 2000; Kuhl and Crisfield 1999; Kuhl and Ramm 1999], which are all included in an enhanced version of the generalized energy momentum method (the so-called GEMM+ $\xi$  method) developed by Kuhl and Crisfield [1999]. Basically,

the only difference between the GEMM+ $\xi$  method and the generalized- $\alpha$  method is the way the internal forces are evaluated—or more specifically, the way for computing a generalized midpoint strain quantity.

In the following, we apply the generalized- $\alpha$  scheme for first-order ODEs formulated as a one-step method to the semidiscrete heat equation (10)<sub>2</sub>. Based on the algorithmic parameter set introduced in (36), whereas  $\beta$  is not used anymore, we violate the criterion of an optimized numerical dissipation in case of the generalized- $\alpha$  for first-order ODEs [Jansen et al. 2000; Rang 2013a; 2013b]. Due to this coupling, the optimal condition for  $\alpha_m$  cannot be satisfied anymore. However, unconditional stability and second-order accuracy for the multistep version are still maintained. We start again with identical linear interpolation rules for the generalized mid-point temperature quantities

$$\Theta_{n+\alpha_f} = \alpha_f \Theta_{n+1} + (1 - \alpha_f) \Theta_n, \quad \dot{\Theta}_{n+\alpha_m} = \alpha_m \dot{\Theta}_{n+1} + (1 - \alpha_m) \dot{\Theta}_n. \quad (45)$$

The discrete temperature velocities  $\dot{\Theta}_{n+1}$  at  $t = t_{n+1}$  can be expressed as

$$\dot{\Theta}_{n+1} = \frac{1}{\gamma \Delta t_n} (\Theta_{n+1} - \Theta_n) - \frac{1-\gamma}{\gamma} \dot{\Theta}_n. \quad (46)$$

Due to the properties of the heat capacity matrix  $\mathbf{C}_\Theta$ , the semidiscrete heat equation (10)<sub>2</sub> can be transformed into explicit form. Applying the generalized- $\alpha$  method yields

$$\dot{\Theta}_{n+\alpha_m} = \mathbf{C}_\Theta^{-1}(\mathbf{U}_{n+\alpha_f}, \Theta_{n+\alpha_f}) \mathbf{r}_\Theta(T_{n+\alpha_f}, \mathbf{U}_{n+\alpha_f}, \dot{\mathbf{U}}_{n+\alpha_f}, \Theta_{n+\alpha_f}, \mathbf{Q}_{n+\alpha_f}), \quad (47)$$

with a capacity matrix evaluated at  $T_{n+\alpha_f}$  (see [Jansen et al. 2000] for further explanation).

In order to apply the same material and element subroutines, we transfer (47) to a DIRK similar structure. By transforming (45)<sub>1</sub> to

$$\Theta_{n+1} = \frac{1}{\alpha_f} \Theta_{n+\alpha_f} - \frac{1-\alpha_f}{\alpha_f} \Theta_n, \quad (48)$$

and substituting into (45)<sub>2</sub>, we arrive at

$$\dot{\Theta}_{n+\alpha_m} = \frac{1}{\Delta t_\alpha} (\Theta_{n+\alpha_f} - \Theta_{n+\alpha_f}^S), \quad (49)$$

with the abbreviation  $\Delta t_\alpha = \alpha_f \gamma \Delta t_n / \alpha_m$  for a time-step quantity and the starting value

$$\Theta_{n+\alpha_f}^S = \Theta_n + \left( \alpha_f - \gamma \frac{\alpha_f}{\alpha_m} \right) \Delta t_n \dot{\Theta}_n = \Theta_n + \frac{\alpha_m - \gamma}{\gamma} \Delta t_\alpha \dot{\Theta}_n, \quad (50)$$

which depends only on already calculated quantities at time  $t_n$ . Finally, we obtain the discrete formulation

$$\begin{aligned} \mathbf{G}_\Theta(t_{n+1}, \mathbf{u}_{n+1}, \Theta_{n+1}, \mathbf{q}_{n+1}) &= \mathbf{C}_\Theta(\mathbf{U}_{n+\alpha_f}, \Theta_{n+\alpha_f}) (\Theta_{n+\alpha_f} - \Theta_{n+\alpha_f}^S) \\ &\quad - \Delta t_\alpha \mathbf{r}_\Theta(T_{n+\alpha_f}, \mathbf{U}_{n+\alpha_f}, \dot{\mathbf{U}}_{n+\alpha_f}, \Theta_{n+\alpha_f}, \mathbf{Q}_{n+\alpha_f}) = \mathbf{0} \end{aligned} \quad (51)$$

of the weak formulation in (9). Analogously to the just considered first-order ODE, the generalized- $\alpha$  method applied to the evolution equations for the internal variables (10)<sub>3</sub> can be written as

$$\mathbf{L}(t_{n+1}, \mathbf{u}_{n+1}, \Theta_{n+1}, \mathbf{q}_{n+1}) = \mathbf{Q}_{n+\alpha_f} - \mathbf{Q}_{n+\alpha_f}^S - \Delta t_\alpha \mathbf{r}_Q(T_{n+\alpha_f}, \mathbf{U}_{n+\alpha_f}, \Theta_{n+\alpha_f}, \mathbf{Q}_{n+\alpha_f}) = \mathbf{0}, \quad (52)$$

with the starting value

$$\mathbf{Q}_{n+\alpha_f}^S = \mathbf{q}_n + \left( \alpha_f - \gamma \frac{\alpha_f}{\alpha_m} \right) \Delta t_n \dot{\mathbf{q}}_n = \mathbf{q}_n + \frac{\alpha_m - \gamma}{\gamma} \Delta t_\alpha \dot{\mathbf{q}}_n. \quad (53)$$

The derivative  $\dot{\mathbf{q}}_{n+1}$  at  $t = t_{n+1}$  is defined, analogously to (46), by

$$\dot{\mathbf{q}}_{n+1} = \frac{1}{\gamma \Delta t_n} (\mathbf{q}_{n+1} - \mathbf{q}_n) - \frac{1-\gamma}{\gamma} \dot{\mathbf{q}}_n. \quad (54)$$

In other words, at each point in time, we have to solve the nonlinear system of equations

$$\begin{aligned} \mathbf{G}_u(\mathbf{u}, \Theta, \mathbf{q}) &= \mathbf{0}, \\ \mathbf{G}_\Theta(\mathbf{u}, \Theta, \mathbf{q}) &= \mathbf{0}, \\ L_Q(\mathbf{u}, \Theta, \mathbf{q}) &= \mathbf{0}, \end{aligned} \quad (55)$$

where we have omitted the time  $t_{n+1}$  and the index  $n+1$  for brevity. One drawback of the procedure can be seen in (54), because we need the derivatives of the quantities at time  $t = 0$ . These can be obtained by evaluating (10) at the beginning of the entire computation.

**3.3. Time adaptivity.** Step-size control is an essential issue to obtain both accurate results and efficient computations. We draw on the approach in [Gustafsson 1994; Hairer et al. 1993; Hairer and Wanner 1996], by using a PI-controller approach. Furthermore, the physical meaning of the different quantities is taken into account. For details, especially for the case of the generalized- $\alpha$  method, see Appendix B.

## 4. Examples

In this section, the performance of the presented algorithms is studied by means of several numerical examples. To demonstrate the advantages and capabilities of the approach in a thermoviscoplastic finite element analysis, two different three-dimensional cases are investigated in detail. The finite element analyses are carried out using the in-house code Tasafem for monolithic, coupled and time-adaptive simulations.

**4.1. Order analysis.** In the first example, we perform an order analysis drawing on a uniaxial tensile specimen, where only one-eighth of the thermoviscoplastic steel specimen is discretized (symmetry conditions are assumed for the displacement as well as temperature distribution, see Figure 3 (left)). For the spatial discretization, we employ a mesh with  $n_{\text{el}} = 360$  twenty-noded hexahedral finite elements ( $p = 2$ ) consisting of a total number  $n_p = 2089$  nodes ( $n_{\text{uu}} = 4803$ ,  $n_{\Theta u} = 2089$ ,  $n_Q = n_{\text{el}} \times 27 \times 12 = 116640$ ), see Figure 3 (left) for the mesh.

The specimen is loaded by a sinusoidal displacement-control at the middle cross-section ( $y = 0$ ) with  $\bar{u}_y = \hat{u} \sin(2\pi f t)$ ,  $\hat{u} = 0.2$  mm,  $f = 10$  Hz within the time interval  $t \in [0 \text{ s}, 0.1 \text{ s}]$ . Starting from the rest position, we choose initial conditions  $\mathbf{u}^h(\mathbf{x}, 0) = \mathbf{0}$ , and  $\Theta^h(\mathbf{x}, 0) = \Theta_0$ , with an initial temperature of  $\Theta_0 = 25$  °C. To ensure consistent initial conditions in the coupled field equations for the velocity and acceleration fields, we apply a smoothing step function (polynomial of fifth order) for  $\bar{u}_y(t)$  within  $t \in [0 \text{ s}, 0.0125 \text{ s}]$  for which  $\mathbf{v}^h(\mathbf{x}, 0) = \mathbf{0}$  and  $\mathbf{a}^h(\mathbf{x}, 0) = \mathbf{0}$  holds, see Figure 3 (right).

The chosen unit system consists of the basic units mm, t, s, and K. The material parameters used in this example can be found in Table 4, where the heat capacity  $c_p$  is given according to the unit



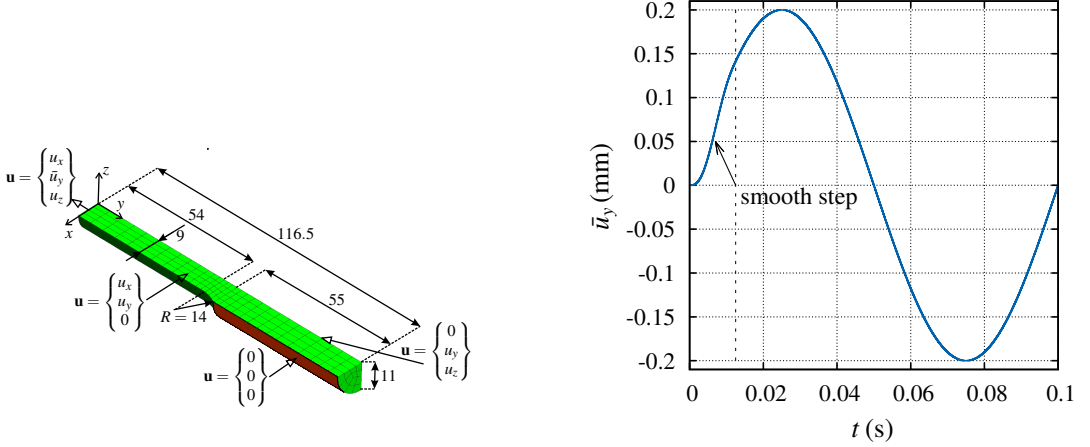


**Figure 3.** Model setup: (left) geometry, mesh and boundary conditions (units in mm); (right) loading path.

material parameters	symbol	value	unit
bulk modulus	$K$	$1.6666 \cdot 10^5$	$\text{N/mm}^2$
change of $K$ with temperature	$c_K$	91	$\text{N}/(\text{mm}^2\text{K})$
shear modulus	$G$	$0.769 \cdot 10^5$	$\text{N/mm}^2$
change of $G$ with temperature	$c_G$	42	$\text{N}/(\text{mm}^2\text{K})$
thermal exp. coef.	$\alpha_\Theta$	$1.2 \cdot 10^{-5}$	$\text{K}^{-1}$
hardening parameter	$c_X$	4230	$\text{N/mm}^2$
hardening parameter	$\beta$	$3 \cdot 10^{-3}$	$\text{N}^{-1}\text{mm}^{-2}$
initial yield stress	$k_0$	450	$\text{N/mm}^2$
yield stress at high temperature	$k_H$	100	$\text{N/mm}^2$
yield stress slope	$b$	$4.2 \cdot 10^{-3}$	$\text{C}^{-1}$
viscosity	$\eta$	$6 \cdot 10^4$	s
exponent	$m$	1	-
normalization stress	$\sigma_0$	1	$\text{N/mm}^2$
density	$\rho$	$7.836 \cdot 10^{-9}$	$\text{Ns}^2/\text{mm}^4$

**Table 4.** Thermoviscoplastic material parameters.

system in  $\text{mm}^2/(\text{s}^2\text{K})$ . Thus, the conversion factor between SI units  $\text{J}/(\text{kgK})$  and the chosen system is  $1 \text{ mm}^2/(\text{s}^2\text{K}) = 10^{-6} \text{ J}/(\text{kgK})$ . Instead of choosing the heat capacity given by (5), we choose a temperature-dependent approach that originates from differential scanning calorimetry measurements. In order to take into consideration the phase transformation at higher temperatures, a log-interpolation of the two functions

$$c_{p1}(\Theta) = a_1 e^{a_2 \Theta} + a_3, \quad c_{p2}(\Theta) = a_4 e^{-a_5(\Theta - \tilde{\Theta}_0)} + a_6 \Theta, \quad (56)$$

<u>abbreviation</u>	<u>method</u>	<b>DIRK</b>		<u>reference</u>
		<u>order</u> $p$	<u>stages</u> $s$	
BE	Backward Euler	1	1	[Butcher 2008]
Alex2/Ell	Alexander/Ellsiepen	2	2	[Alexander 1977; Ellsiepen 1999]
CAA	trapezoidal rule or CAA	2	2	[Hughes 1987; Ellsiepen and Hartmann 2001]
Alex3/Cash	Alexander/Cash	3	3	[Alexander 1977; Cash 1979]
CAA+BE	CAA + Backward Euler	2/1	2/1	-

<u>abbreviation</u>	<u>method</u>	<b>generalized-<math>\alpha</math></b>		<u>reference</u>
		<u>order</u> $p$	<u>stages</u> $s$	
Gen- $\alpha$	generalized- $\alpha$ , $\rho_\infty = 0.8$	2	-	[Chung and Hulbert 1993]

**Table 5.** Applied one-step methods with references in the context of ODE solution and applications within finite elements.

is chosen according to Kreisselmeier and Steinhauser [1979]

$$c_p(\Theta) = -c_W \ln \left( \frac{e^{-c_{p1}(\Theta)/c_W} + e^{-c_{p2}(\Theta)/c_W}}{2} \right). \quad (57)$$

The calibrated parameters are as follows:  $a_1 = 34.2 \text{ J}/(\text{kgK})$ ,  $a_2 = 0.0026 \text{ K}^{-1}$ ,  $a_3 = 421.15 \text{ J}/(\text{kgK})$ ,  $a_4 = 956.5 \text{ J}/(\text{kgK})$ ,  $a_5 = 0.012 \text{ K}^{-1}$ ,  $a_6 = 0.45 \text{ K}/(\text{kgK}^2)$ , and  $\Theta_0 = 900 \text{ K}$ . The weighting factor of the interpolation function is chosen to be  $c_W = 30 \text{ J}/(\text{kgK})$ .

The thermal conductivity  $\kappa$  is given in  $\text{tmm}/(\text{s}^3\text{K})$ , which is equivalent to  $\text{W}/(\text{mK})$ . According to Quint et al. [2011] we assume

$$\kappa(\Theta) = b_0 + b_1\Theta + b_2\Theta^2 + b_3\Theta^3, \quad (58)$$

with  $b_0 = 40.1 \text{ W}/(\text{mK})$ ,  $b_1 = 0.05 \text{ W}/(\text{mK}^2)$ ,  $b_2 = -10^{-4} \text{ W}/(\text{mK}^3)$ , and  $b_3 = 4.9 \cdot 10^{-8} \text{ W}/(\text{mK}^4)$ , which are taken from the steel 51CrV4.

For the order considerations, the relative error measures of the displacement, velocity, temperature field and internal variables are computed. The relative error quantities are defined by the maximum relative error over all points in time  $t_n$ , given as

$$\mathbf{err}_u = \max_n \left( \frac{\|u_n^{\text{ref}} - u_n\|}{\max_n (\|u_n^{\text{ref}}\|)} \right), \quad \mathbf{err}_v = \max_n \left( \frac{\|v_n^{\text{ref}} - v_n\|}{\max_n (\|v_n^{\text{ref}}\|)} \right), \quad (59)$$

$$\mathbf{err}_\Theta = \max_n \left( \frac{\|\Theta_n^{\text{ref}} - \Theta_n\|}{\max_n (\|\Theta_n^{\text{ref}}\|)} \right), \quad \mathbf{err}_q = \max_n \left( \frac{\|q_n^{\text{ref}} - q_n\|}{\max_n (\|q_n^{\text{ref}}\|)} \right), \quad (60)$$

For the illustrated problem the integration methods compiled in Table 5 are analyzed in view of their expected and achieved temporal convergence order for different fields. For further information regarding the applied DIRK methods, we refer to [Ellsiepen and Hartmann 2001] and the literature cited in Table 5. Cash's [1979] method is the time-adaptive extension using an embedded scheme of Alexander's [1977]

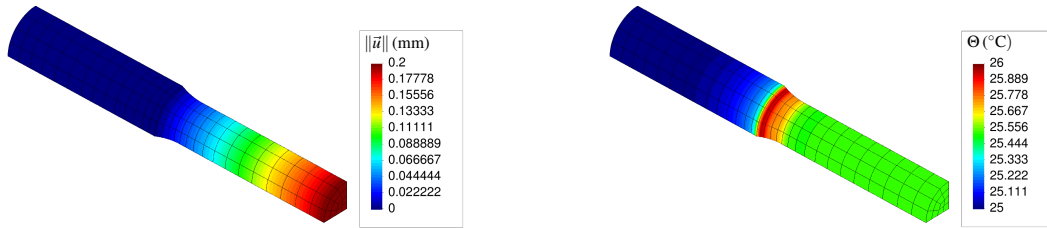


**Figure 4.** Displacement norm (left) and temperature distribution (right) for reference solution (Alex3/Cash,  $\Delta t_n = 10^{-5}$  s) at  $t = 0.075$  s.

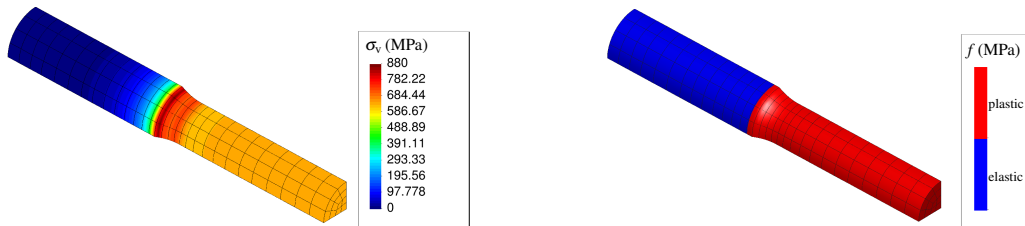


**Figure 5.** von Mises-stress distribution (left) and yield function state (right) for reference solution (Alex3/Cash,  $\Delta t_n = 10^{-5}$  s) at  $t = 0.075$  s.

method of third order. Similarly, Ellsiepen’s [1999] method is the time-adaptive extension of Alexander’s [1977] second-order method. In the following we call them Alex3/Cash and Alex2/Ell.

The algorithmic parameters of the generalized- $\alpha$  method —  $\alpha_f$ ,  $\alpha_m$ ,  $\beta$  and  $\gamma$  — are computed using (36) as function of the spectral radius  $\rho_\infty$ . The order of convergence is given by the slope of the curves in a double logarithmic plot. The reference solution is given by Alex3/Cash (highest-order method of our investigations), with a constant step-size of  $\Delta t_n = 10^{-5}$  s. The resulting deformation and temperature distribution for the reference solution at  $t = 0.075$  s are shown in Figure 4. Mechanical agencies of the structure change the temperature distribution due to plastic dissipation, and cause plastic deformations, see Figure 5.

Regarding the order considerations for the displacement field, only the Backward Euler (which is the simplest DIRK method), the applied Newmark-scheme in the parametrization of the trapezoidal rule (CAA), and the generalized- $\alpha$  method reach their theoretical orders in Figure 6 (left). The convergence order for Alex2/Ell and Alex3/Cash degenerates after passing an optimal step-size. The reasons for this are not known.

Due to the strong coupling of the displacement field to the internal variables, the combination of the CAA and Backward Euler methods yields only order one, i.e., the order of the global trapezoidal rule (Newmark-scheme) will be reduced, and the artificially created order reduction in the internal variables affects the order in the displacement field. Thus, commercial programs using the Newmark-method combined with a Backward Euler-like scheme on Gauss-point level for integrating the internal variables cannot reach second order. This is different in the pure CAA approach.

For the convergence behavior in the velocity field, the higher-order DIRK methods — excluding the Newmark-type schemes (CAA, generalized- $\alpha$  method) — reach only first order (see Figure 6 (right)).

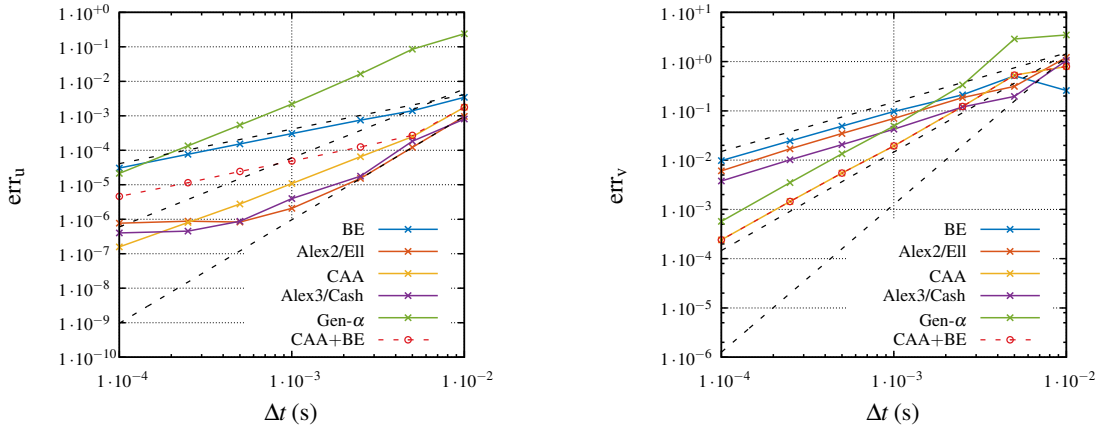


**Figure 6.** Convergence behavior for order analysis: (left) global error in displacement field and (right) global error in velocity field.

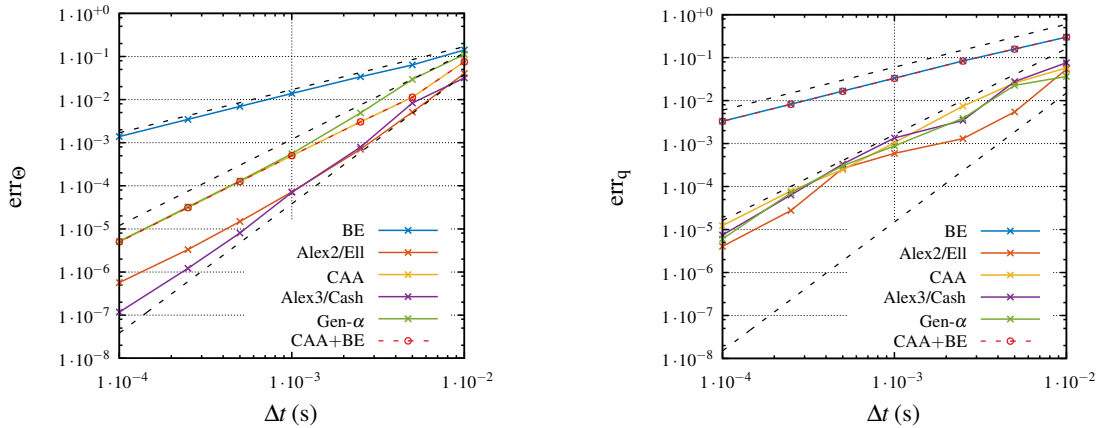


**Figure 7.** Convergence behavior for order analysis: (left) global error in temperature field and (right) global error for internal variables.

However, the field variable velocity is only of minor importance compared to the others. On the other hand, the convergence behavior for the temperature field in [Figure 7](#) (left) for the different time integration methods matches the theory. As reported in [[Ellsiepen 1999](#); [Ellsiepen and Hartmann 2001](#)], we observe in the convergence graph for the internal variables ([Figure 7](#) (right))—due to the lack of smoothness in the time domain—an order reduction where the third order of the Alex3/Cash method is not attained. This is known from quasistatic and isothermal computations [[Ellsiepen and Hartmann 2001](#)]. As already mentioned, the combination of Backward Euler for the internal variables (stress-algorithm) and the Newmark-method yields only order one.

It is not only the rate of convergence that is of practical importance, but the computational costs of the methods as well. [Figures 8](#) and [9](#) show the relative error in each field variable versus the computational time.

In these plots, the second-order DIRK methods (Alex2/Ell, CAA), with the exception of [Figure 8](#) (right), show an identical slope, which is steeper than the more accurate Alex3/Cash-method. They are more

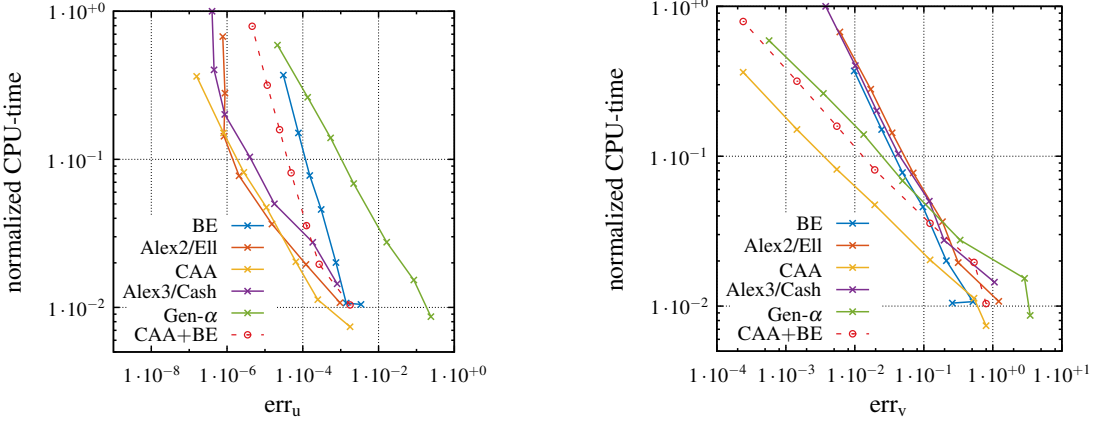


**Figure 8.** Efficiency analyses for displacement (left) and velocity (right) fields.

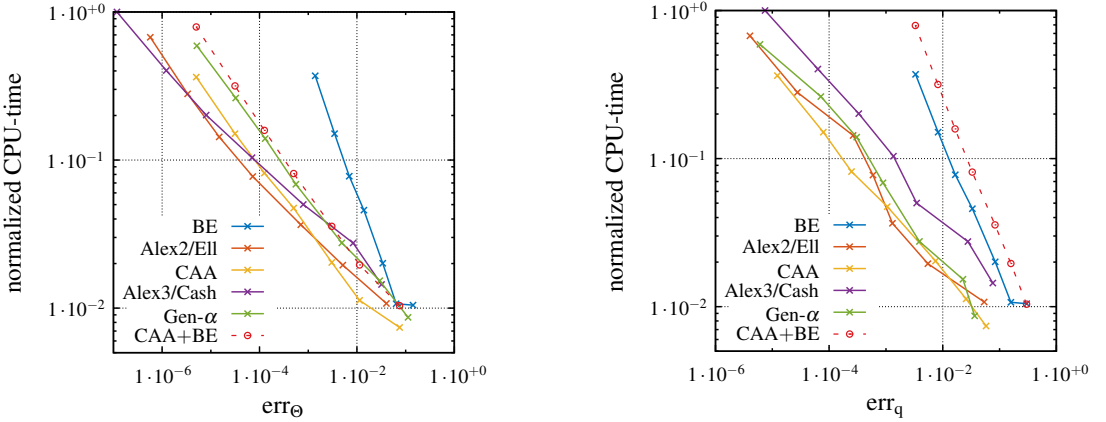


**Figure 9.** Efficiency analyses for temperature field (left) and internal variables (right).

efficient for high accuracy requirements, i.e., the fastest methods for a given error tolerance. The Backward Euler method yields only comparatively rough results—even for high computational times. The considered generalized- $\alpha$  method behaves only moderately: acceptable results are only obtained for the smallest time-step, see Figure 8 (left). All in all, the combination of Newmark-method and Backward Euler seems to be superior to the pure Backward Euler method, but is not as attractive as the generalized- $\alpha$  method due to the small slope in the displacements.

We would like to remark that the increase of elements by a factor of two in all directions, which yields more accurate results in the spatial domain, does not influence the order diagrams, especially the order reduction phenomenon of CAA and Alex3/Cash in Figure 6 (left). This can be explained by the accuracy of the error tolerance of the global MLNA step, where the tolerances (norm of  $\Delta \mathbf{u}$  and  $\Delta \boldsymbol{\Theta}$ ) could not be smaller than  $10^{-7}$  in the computations. Otherwise, the MLNA will not converge.

**4.2. H-Beam.** In the second example, we study the dynamical behavior of a thermoviscoplastic H-Beam profile by performing time-adaptive computations. The error of the current time-step is estimated by using embedding methods as described in Section 3.3. The dimensions of the profile are depicted in

$\varepsilon_a^u$	$\varepsilon_r^u$	$\varepsilon_a^\Theta$	$\varepsilon_r^\Theta$	$\varepsilon_a^q$	$\varepsilon_r^q$
$1.0 \cdot 10^{-2}$ mm	$1.0 \cdot 10^{-3}$	$1.0 \cdot 10^{-2}$ °C	$1.0 \cdot 10^{-3}$	$1.0 \cdot 10^{-5}$	$1.0 \cdot 10^{-5}$

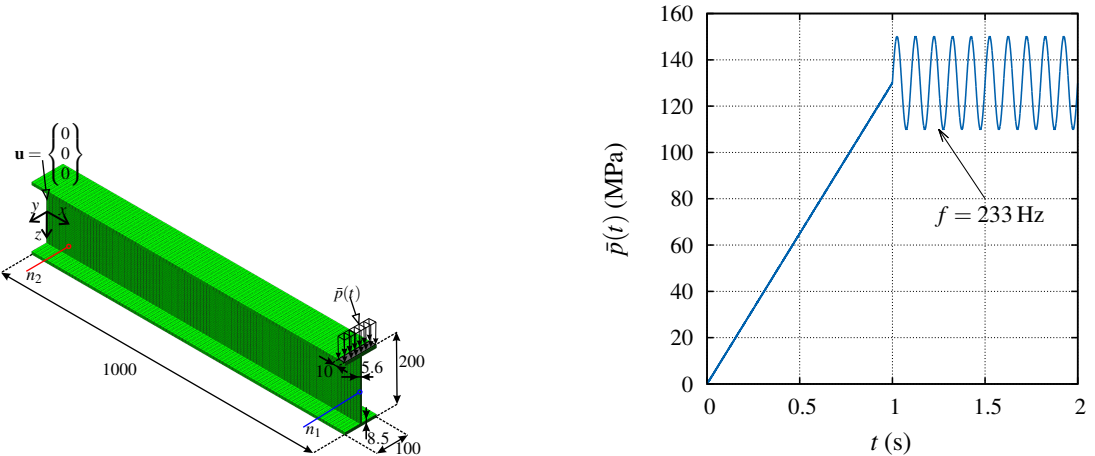
**Table 6.** Absolute and relative error tolerances for step-size estimation.

Figure 10 (left) and the material parameters are given in Table 4 with the nonlinear material functions (57) and (58). The left end of the beam is clamped, i.e., all displacements are fixed, and the right side is loaded by a time-dependent cyclic pressure load in  $z$ -direction,

$$\bar{p}(t) = \begin{cases} K_p t & \text{for } 0 \leq t \leq 1 \text{ s with } K_p = 130 \text{ MPa/s} \\ p_0 \sin(2\pi f t) & \text{for } 1 \text{ s} < t \leq 2 \text{ s with } p_0 = 20 \text{ MPa, } f = 233 \text{ Hz} \end{cases} \quad (61)$$

see Figure 10 (right). The frequency is chosen to be close to an eigenfrequency so that the influence of the inertia terms becomes larger. Similar computations — which are not shown here — at a loading frequency of  $f = 60$  Hz show very similar amplitudes and phases for all time integration schemes. This holds for the step-size behavior as well. The whole profile is discretized with  $n_{el} = 11200$  twenty-noded hexahedral finite elements. Consequently, this implies a total number of 68591 nodes ( $n_{uu} = 204300$ ,  $n_{\Theta u} = 68591$ ) with  $n_Q = n_{el} \times 27 \times 12 = 3628800$  internal variables. The problem setup is completed by the initial conditions  $\mathbf{u}^h(\mathbf{x}, 0) = \mathbf{0}$ ,  $\mathbf{v}^h(\mathbf{x}, 0) = \mathbf{0}$ ,  $\mathbf{q}(0) = \mathbf{0}$ , and initial temperature distribution  $\Theta^h(\mathbf{x}, 0) = \Theta_0$  with reference temperature  $\Theta_0 = 25$  °C.

For all investigated time-integration methods, namely the generalized- $\alpha$  (Gen- $\alpha$ ), Newmark (CAA), and Ellsiepen (Alex2/Ell) time integrators, the same absolute and relative error tolerances for the field variable’s displacement, temperature and internal variables are used (see Table 6) in order to estimate the new step-sizes. The proposed adaptive time-step control uses the error measure  $e_m = \max(e_u, e_v, e_\theta, e_q)$  for the step-size selection rule (95). As a result of the observed poor convergence behavior in the velocity field for the DIRK methods Alex2/Ell and Alex3/Cash (see Figure 6 (right)), we do not take  $e_v$  into account to compute  $e_m$ . This — in combination with the chosen factors  $f_{\min} = 0.3$ ,  $f_{\max} = 2.5$ , and



**Figure 10.** Model setup and loading process: dimensions of the H-Beam, mesh and boundary conditions (units in mm) (left); schematic loading path (right).

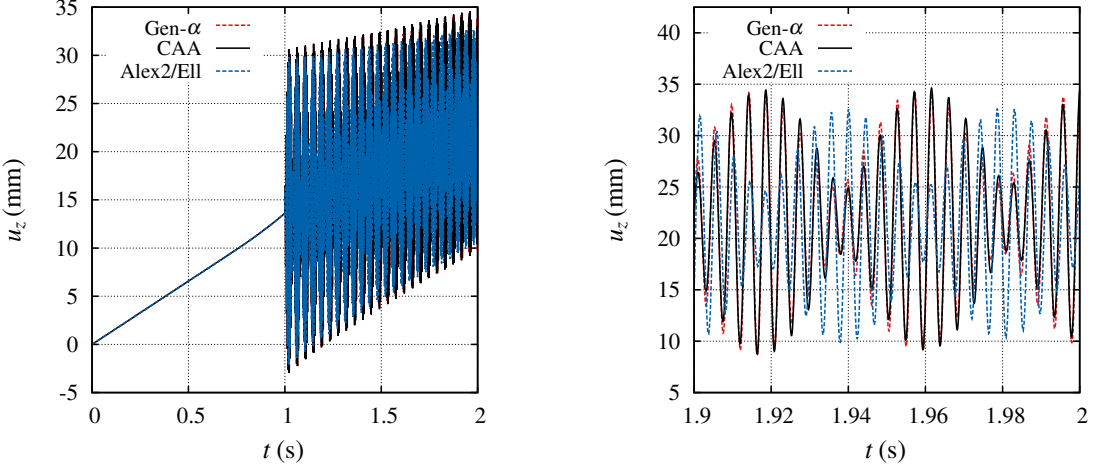


**Figure 11.** Displacement result for evaluation point  $n_1$  of Figure 10: deflection in  $z$ -direction ( $0 \leq t \leq 2$  s) (left); deflection in  $z$ -direction (subinterval  $1.9 \text{ s} \leq t \leq 2$  s) (right).

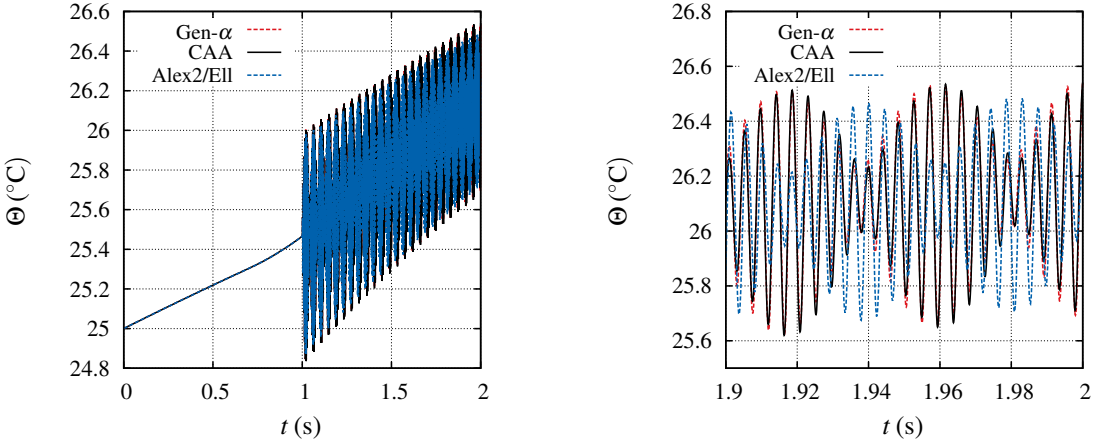


**Figure 12.** Temperature results for evaluation point  $n_2$  shown in Figure 10: temperature evolution ( $0 \leq t \leq 2$  s) (left); temperature evolution (subinterval  $1.9 \text{ s} \leq t \leq 2$  s) (right).

$f_{\text{safety}} = 0.85$  of the step-size controller — leads to the step-size behavior shown in Figure 15 (left). An initial step-size of  $\Delta t_0 = 10^{-2} \text{ s}$  is chosen and applied at each external load-change, i.e., at  $t_n = 0 \text{ s}$  and  $t_n = 1 \text{ s}$ . In the quasistatic loading range the step-size increases until it is limited by the stability of the employed Multilevel Newton algorithm. If there are time-steps that are too large, a failure of the applied Newton algorithm on the local level is obtained. Thus, step-size rejections are observable. As the dynamics of higher modes of the structure are stimulated by the cyclic loading, the step-size in this time interval is reduced significantly by the time-adaptive scheme.

For a comparison of the integration schemes, we consider the structural response at two nodes  $n_1$  and  $n_2$ . Figure 11 shows the deflection/time behavior at node  $n_1$ . At the second evaluation point  $n_2$ , however, we observe the temperature evolution depicted in Figure 12. The generalized- $\alpha$  method and the applied Newmark-scheme (CAA) yield approximately the same structural response, see Figure 11 (right) and

Method	No. of time-steps	CPU time (s)	Efficiency factor
Gen- $\alpha$	12592	253136	0.54
CAA	12601	467034	1.00
Alex2/Ell	4107	106077	0.23

**Table 7.** Computational costs of applied time integration schemes.

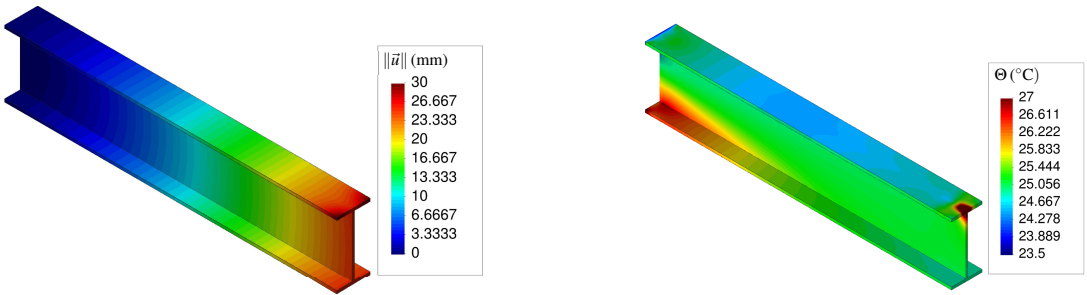


**Figure 13.** Displacement (left) and temperature (right) distribution at the end of the computation ( $t = 2$  s), computed with Ellsiepen’s method.

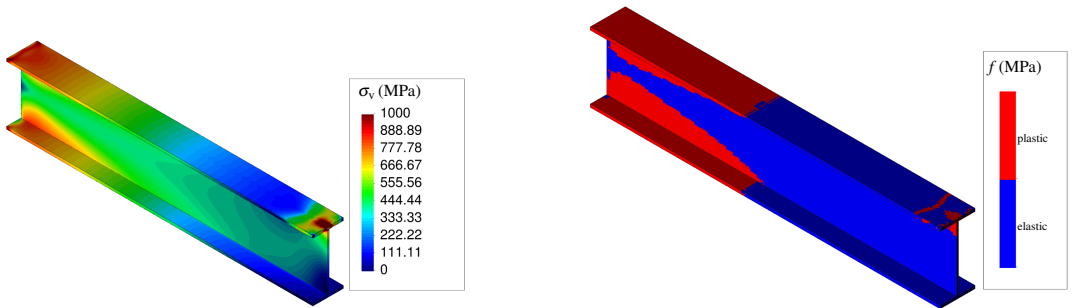


**Figure 14.** von Mises stress (left) and yield function (right) state at the end of the computation ( $t = 2$  s), computed with Ellsiepen’s method.

Figure 12 (right). Moreover, both show a very similar step-size behavior which can be observed in Figure 15. However, as shown by the CPU times in Table 7, the generalized- $\alpha$  requires only 54% of the computational time of the trapezoidal rule (CAA). This fact is due to the use of a further stage in the embedded scheme for the trapezoidal rule (a Backward Euler stage) for applying the proposed time-adaptivity procedure in Section 3. The generalized- $\alpha$  method uses an estimation introduced by Rang [2013a; 2013b]. Ellsiepen’s method yields larger step-sizes in the cyclic loading range and, accordingly, leads to the fastest computation.

Figures 13 and 14 (left) show the displacement, temperature and von Mises stress distribution at the final stage of a time-adaptive computation with the Ellsiepen integrator. In Figure 14 (right), we consider the regions where yielding appears. When the cyclic load is applied, a plastic zone starts to evolve at the upper and the lower surface of the clamping. One can clearly see that in the area of clamping — above and



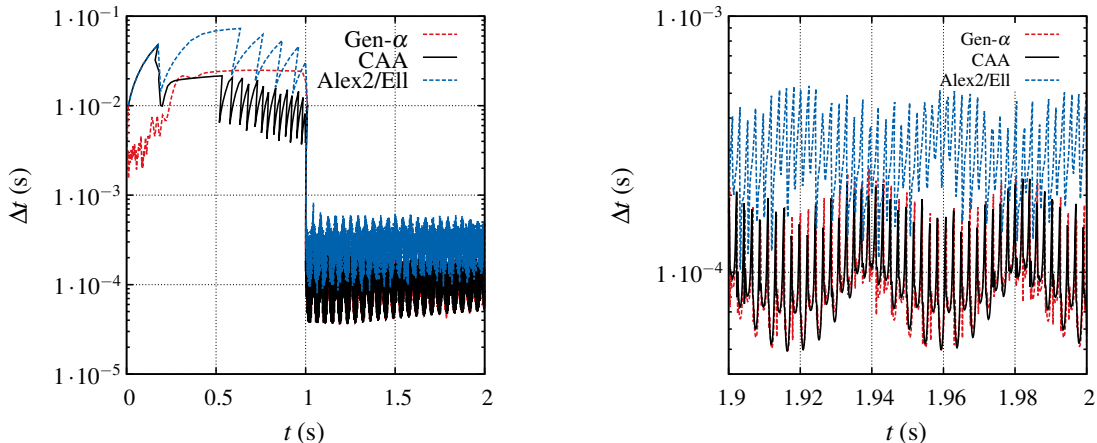


**Figure 15.** Step-size behavior: (left)  $0 \text{ s} \leq t \leq 2 \text{ s}$ ; (right) subinterval  $1.9 \text{ s} \leq t \leq 2 \text{ s}$ .

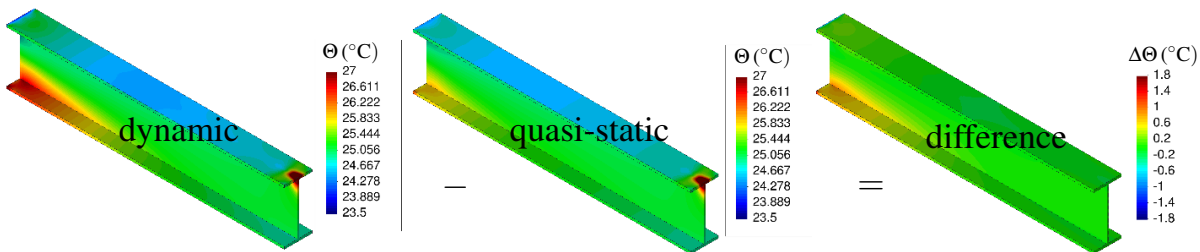


**Figure 16.** Temperature difference between dynamic and quasistatic computation at the end of the computation ( $t = 2 \text{ s}$ ), computed with Ellsiepen's method.

below, where a singularity exists — the highest stresses occur. Furthermore, due to the elastic coupling effect in the constitutive model, the maximum temperature occurs in the lower part of the clamping.

Figure 16 shows the influence of the inertia terms on the temperature distribution by comparing a dynamical simulation with a quasistatic one. For this purpose, we perform an identical quasistatic simulation by ignoring the inertia term and computing the difference between both simulations. The resulting DAE system of the quasistatic simulation is listed in (14). It can clearly be seen that in the lower part of the clamping, the temperature differs and reveals a temperature increase. In the remaining part of the structure, there is no drastic change in temperature.

## 5. Conclusions

We studied the resulting ODE system of dynamical problems which were combined with heat conduction problems and inelastic material behavior. All equations are coupled. The problem under consideration is related to the computation of a system of second-order ODEs with first-order ODEs. The classical Newmark-method, which is a method of second-order combined with stress-algorithms of first order on Gauss-point level, does not lead to a second-order scheme. Thus, other methods must be treated. Another

question is connected to an automatic step-size control technique based on local error estimations, due to which the physical quantities and their temporal evolution determine the step-size.

Apart from the compilation of different semidiscrete forms, we investigated stiffly accurate, diagonally implicit Runge–Kutta methods and the generalized- $\alpha$  method (single-step version). In the case of DIRK methods, the second-order ODE part is transformed into a system of first-order ODEs. A particular discussion of the relation to Runge–Kutta–Nyström methods was offered as well. The generalized- $\alpha$  method, originally developed for second-order ODEs, was combined with a generalized- $\alpha$  method for first-order ODEs. The different schemes were studied in view of their order of accuracy revealing similar behavior. Since an order-reduction is known for the case of yield function-based models, only second-order accuracy was expected. This was obtained for all methods in the displacements, temperatures and internal variables. Only the fully consistently applied trapezoidal scheme (CAA)—consistent with the integration scheme on Gauss-point level to determine the internal variables—the expected order is achieved in the velocities as well.

Additional investigations of the embedded time-step control of the DIRK methods and the generalized- $\alpha$  methods proved both the applicability of the time-adaptivity of the two methods as well as the greater efficiency of DIRK methods. Unfortunately, the fully consistent CAA method is computationally four times slower than the DIRK approach in our examples. Thus, either Ellsiepen’s method, which has turned out to be very efficient for quasistatic and coupled problems, or the generalized- $\alpha$  should be applied. The latter method is also applicable for problems with internal variables if it is applied in a consistent manner. However, there is the drawback that the function evaluations are at stage-times within a time-interval so that constraint problems cannot be satisfied.

### Appendix A. Derivation of matrices

In this section, we draw on the notation used in [Rothe et al. 2015a]. In finite elements, the displacements  $\vec{u}(\vec{x}, t)$ , the virtual displacements  $\delta\vec{u}(\vec{x})$ , the temperatures  $\Theta(\vec{x}, t)$ , and the virtual temperatures  $\delta\Theta(\vec{x})$  are approximated by shape functions within an element  $e$ ,

$$\mathbf{u}^h(\mathbf{x}, t) = \mathbf{N}_u^e(\boldsymbol{\varphi}_u^e(\mathbf{x}))\mathbf{u}^e(t) = \mathbf{N}_u^e(\boldsymbol{\varphi}_u^e(\mathbf{x}))\mathbf{Z}_{ua}^e\mathbf{U}_a = \mathbf{N}_u^e(\boldsymbol{\varphi}_u^e(\mathbf{x}))\{\mathbf{Z}_u^e\mathbf{u} + \bar{\mathbf{Z}}_u^e\bar{\mathbf{u}}(t)\}, \quad (62)$$

$$\dot{\mathbf{u}}^h(\mathbf{x}, t) = \mathbf{N}_u^e(\boldsymbol{\varphi}_u^e(\mathbf{x}))\dot{\mathbf{u}}^e(t) = \mathbf{N}_u^e(\boldsymbol{\varphi}_u^e(\mathbf{x}))\mathbf{Z}_{ua}^e\dot{\mathbf{U}}_a = \mathbf{N}_u^e(\boldsymbol{\varphi}_u^e(\mathbf{x}))\{\mathbf{Z}_u^e\dot{\mathbf{u}} + \bar{\mathbf{Z}}_u^e\dot{\bar{\mathbf{u}}}(t)\}, \quad (63)$$

$$\ddot{\mathbf{u}}^h(\mathbf{x}, t) = \mathbf{N}_u^e(\boldsymbol{\varphi}_u^e(\mathbf{x}))\ddot{\mathbf{u}}^e(t) = \mathbf{N}_u^e(\boldsymbol{\varphi}_u^e(\mathbf{x}))\mathbf{Z}_{ua}^e\ddot{\mathbf{U}}_a = \mathbf{N}_u^e(\boldsymbol{\varphi}_u^e(\mathbf{x}))\{\mathbf{Z}_u^e\ddot{\mathbf{u}} + \bar{\mathbf{Z}}_u^e\ddot{\bar{\mathbf{u}}}(t)\}, \quad (64)$$

$$\delta\mathbf{u}^h(\mathbf{x}) = \mathbf{N}_u^e(\boldsymbol{\varphi}_u^e(\mathbf{x}))\delta\mathbf{u}^e = \mathbf{N}_u^e(\boldsymbol{\varphi}_u^e(\mathbf{x}))\mathbf{Z}_{ua}^e\delta\mathbf{U}_a = \mathbf{N}_u^e(\boldsymbol{\varphi}_u^e(\mathbf{x}))\mathbf{Z}_u^e\delta\mathbf{u}, \quad (65)$$

$$\Theta^h(\mathbf{x}, t) = \mathbf{N}_\Theta^e(\boldsymbol{\varphi}_\Theta^e(\mathbf{x}))\Theta^e(t) = \mathbf{N}_\Theta^e(\boldsymbol{\varphi}_\Theta^e(\mathbf{x}))\mathbf{Z}_{\Theta a}^e\Theta_a = \mathbf{N}_\Theta^e(\boldsymbol{\varphi}_\Theta^e(\mathbf{x}))\{\mathbf{Z}_\Theta^e\Theta + \bar{\mathbf{Z}}_\Theta^e\bar{\Theta}(t)\}, \quad (66)$$

$$\dot{\Theta}^h(\mathbf{x}, t) = \mathbf{N}_\Theta^e(\boldsymbol{\varphi}_\Theta^e(\mathbf{x}))\dot{\Theta}^e(t) = \mathbf{N}_\Theta^e(\boldsymbol{\varphi}_\Theta^e(\mathbf{x}))\mathbf{Z}_{\Theta a}^e\dot{\Theta}_a = \mathbf{N}_\Theta^e(\boldsymbol{\varphi}_\Theta^e(\mathbf{x}))\{\mathbf{Z}_\Theta^e\dot{\Theta} + \bar{\mathbf{Z}}_\Theta^e\dot{\bar{\Theta}}(t)\}, \quad (67)$$

$$\delta\Theta^h(\mathbf{x}) = \mathbf{N}_\Theta^e(\boldsymbol{\varphi}_\Theta^e(\mathbf{x}))\delta\Theta^e = \mathbf{N}_\Theta^e(\boldsymbol{\varphi}_\Theta^e(\mathbf{x}))\mathbf{Z}_{\Theta a}^e\delta\Theta_a = \mathbf{N}_\Theta^e(\boldsymbol{\varphi}_\Theta^e(\mathbf{x}))\mathbf{Z}_\Theta^e\delta\Theta, \quad (68)$$

where  $\mathbf{u}^h \in \mathbb{R}^3$ ,  $\delta\mathbf{u}^h \in \mathbb{R}^3$ . For the three-dimensional case we have the matrix and vector shape functions  $\mathbf{N}_u^e \in \mathbb{R}^{3 \times n_u^e}$ , and  $\mathbf{N}_\Theta^e \in \mathbb{R}^{n_\Theta^e}$ , where  $n_u^e$  and  $n_\Theta^e$  are the displacement and temperature element degrees of freedom (DOF). Here,  $\mathbf{u}^e \in \mathbb{R}^{n_u^e}$  and  $\Theta^e \in \mathbb{R}^{n_\Theta^e}$  describe the element DOF. In the case of  $h$ -elements, these are displacements and nodal temperatures. The expression  $\boldsymbol{\xi} = \boldsymbol{\varphi}_u^e(\mathbf{x})$  defines the inverse coordinate transformation of the global coordinates  $\mathbf{x}$  to the local coordinates  $\boldsymbol{\xi}$  in the reference element. Here, we have

to distinguish between the coordinate transformation  $\boldsymbol{\varphi}_u^e$  in the mechanical problem and the coordinate transformation in the thermal problem  $\boldsymbol{\xi} = \boldsymbol{\varphi}_\Theta^e(\mathbf{x})$ . In a monolithic approach, both transformations are assumed to be identical,  $\boldsymbol{\varphi}_u^e(\mathbf{x}) = \boldsymbol{\varphi}_\Theta^e(\mathbf{x})$  (of course, a generalization might be possible). In a partitioned approach both meshes can be different. Thus, the given coordinate transformations  $\mathbf{x} = \boldsymbol{\chi}_u^e(\boldsymbol{\xi})$  and  $\mathbf{x} = \boldsymbol{\chi}_\Theta^e(\boldsymbol{\xi})$  with  $\boldsymbol{\chi}_u^e = \boldsymbol{\varphi}_u^{e-1}$  and  $\boldsymbol{\chi}_\Theta^e = \boldsymbol{\varphi}_\Theta^{e-1}$  are distinct in the general case. In this context,  $\mathbf{u}_a \in \mathbb{R}^{n_{ua}}$  symbolizes all displacement DOF for the entire structure containing the unknown quantities  $\mathbf{u} \in \mathbb{R}^{n_{uu}}$  and the known (prescribed) displacement DOF  $\bar{\mathbf{u}} \in \mathbb{R}^{n_{up}}$ . Obviously,  $n_{ua} = n_{uu} + n_{up}$  for  $\mathbf{u}_a^T = \{\mathbf{u}^T \bar{\mathbf{u}}^T\}$  holds. The same decomposition is carried out for the temperature DOF,  $\boldsymbol{\Theta}_a \in \mathbb{R}^{n_{\Theta a}}$ ,  $\boldsymbol{\Theta} \in \mathbb{R}^{n_{\Theta u}}$ ,  $\bar{\boldsymbol{\Theta}} \in \mathbb{R}^{n_{\Theta p}}$  (i.e.,  $\boldsymbol{\Theta}_a^T = \{\boldsymbol{\Theta}^T \bar{\boldsymbol{\Theta}}^T\}$  and  $n_{\Theta a} = n_{\Theta u} + n_{\Theta p}$ ). For  $n_{ij}$  the first index denotes the mechanical and the thermal quantities,  $i = u, \Theta$ . The second subscript,  $j = a, u, p$ , stands for all, unknown and prescribed. The terms  $\bar{\mathbf{u}}(t)$  and  $\bar{\boldsymbol{\Theta}}(t)$  are the given functions at time  $t$  representing displacement-control and prescribed temperature boundary conditions. The incidence matrices  $\mathbf{Z}_u^e \in \mathbb{R}^{n_u^e \times n_{uu}}$ ,  $\bar{\mathbf{Z}}_u^e \in \mathbb{R}^{n_u^e \times n_{up}}$ ,  $\mathbf{Z}_\Theta^e \in \mathbb{R}^{n_\Theta^e \times n_{\Theta u}}$ , and  $\bar{\mathbf{Z}}_\Theta^e \in \mathbb{R}^{n_\Theta^e \times n_{\Theta p}}$  are related to the assemblage procedures, which are frequently symbolized by either  $\bigcup_{e=1}^{n_{el}^\Theta}$  or  $\mathbf{A}_{e=1}^{n_{el}^\Theta}$  in [Wriggers 2001; Hughes 1987]. Accordingly, the incidence matrices  $\mathbf{Z}$  are not programmed explicitly, but symbolize the assemblage procedure of “local” quantities into “global” vectors or matrices. They are also helpful in developing new algorithms [Hartmann 2005; Hartmann and Hamkar 2010] or for describing the transition from local to global quantities.

In view of d’Alembert’s principle (8) and temperatures (9), respectively, both the strain and virtual strain vectors as well as the temperature gradient and virtual temperature gradient are required:

$$\mathbf{E}^e(t, \boldsymbol{\xi}, \mathbf{u}) = \mathbf{B}_u^e(\boldsymbol{\xi}) \mathbf{u}^e(t) = \mathbf{B}_u^e(\boldsymbol{\xi}) \{ \mathbf{Z}_u^e \mathbf{u} + \bar{\mathbf{Z}}_u^e \bar{\mathbf{u}}(t) \}, \quad (69)$$

$$\dot{\mathbf{E}}^e(t, \boldsymbol{\xi}, \dot{\mathbf{u}}) = \mathbf{B}_u^e(\boldsymbol{\xi}) \dot{\mathbf{u}}^e(t) = \mathbf{B}_u^e(\boldsymbol{\xi}) \{ \mathbf{Z}_u^e \dot{\mathbf{u}} + \bar{\mathbf{Z}}_u^e \dot{\bar{\mathbf{u}}}(t) \}, \quad (70)$$

$$\delta \mathbf{E}^e(\boldsymbol{\xi}, \delta \mathbf{u}) = \mathbf{B}_u^e(\boldsymbol{\xi}) \delta \mathbf{u}^e = \mathbf{B}_u^e(\boldsymbol{\xi}) \mathbf{Z}_u^e \delta \mathbf{u}, \quad (71)$$

$$\boldsymbol{\gamma}^e(t, \boldsymbol{\xi}, \boldsymbol{\Theta}) = \text{grad } \Theta^h = \mathbf{B}_\Theta^e(\boldsymbol{\xi}) \boldsymbol{\Theta}^e(t) = \mathbf{B}_\Theta^e(\boldsymbol{\xi}) \{ \mathbf{Z}_\Theta^e \boldsymbol{\Theta} + \bar{\mathbf{Z}}_\Theta^e \bar{\boldsymbol{\Theta}}(t) \}, \quad (72)$$

$$\delta \boldsymbol{\gamma}^e(\boldsymbol{\xi}, \delta \boldsymbol{\Theta}) = \text{grad } \delta \Theta^h = \mathbf{B}_\Theta^e(\boldsymbol{\xi}) \delta \boldsymbol{\Theta}^e = \mathbf{B}_\Theta^e(\boldsymbol{\xi}) \mathbf{Z}_\Theta^e \delta \boldsymbol{\Theta}, \quad (73)$$

where  $\mathbf{B}_u^e(\boldsymbol{\xi}) \in \mathbb{R}^{6 \times n_u^e}$  symbolizes the strain-displacement matrix, and  $\mathbf{B}_\Theta^e(\boldsymbol{\xi}) \in \mathbb{R}^{3 \times n_\Theta^e}$  represents the temperature gradient-temperature matrix. In Voigt-notation, the stresses (1) read  $\mathbf{T} = \mathbf{h}(\mathbf{E}, \boldsymbol{\Theta}, \mathbf{q})$ ,  $\mathbf{T} \in \mathbb{R}^6$ ,  $\mathbf{E} \in \mathbb{R}^6$ , which are inserted into the weak form (8) leading to the second-order ODE

$$\mathbf{M} \ddot{\mathbf{u}}(t) = -\mathbf{g}_u(t, \mathbf{u}, \boldsymbol{\Theta}, \mathbf{q}) - \mathbf{M}_{up} \ddot{\bar{\mathbf{u}}}(t) \quad (74)$$

with

$$\mathbf{g}_u(t, \mathbf{u}, \boldsymbol{\Theta}, \mathbf{q}) = \sum_{e=1}^{n_{el}^u} \mathbf{Z}_u^{eT} \left\{ \sum_{j=1}^{n_{Gpu}^e} w_u^{e(j)} \mathbf{B}_u^{e(j)T} \mathbf{h}(\mathbf{E}^{e(j)}, \Theta^{e(j)}, \mathbf{q}^{e(j)}) \det \mathbf{J}_u^{e(j)} \right\} - \bar{\mathbf{p}}(t), \quad (75)$$

$$\mathbf{M} = \sum_{e=1}^{n_{el}^u} \mathbf{Z}_u^{eT} \left[ \sum_{j=1}^{n_{Gpu}^e} w_u^{e(j)} \mathbf{N}_u^{e(j)T} \mathbf{N}_u^{e(j)} \rho^{e(j)} \det \mathbf{J}_u^{e(j)} \right] \mathbf{Z}_u^e, \quad (76)$$

$$\mathbf{M}_{up} = \sum_{e=1}^{n_{el}^u} \mathbf{Z}_u^{eT} \left[ \sum_{j=1}^{n_{Gpu}^e} w_u^{e(j)} \mathbf{N}_u^{e(j)T} \mathbf{N}_u^{e(j)} \rho^{e(j)} \det \mathbf{J}_u^{e(j)} \right] \bar{\mathbf{Z}}_u^e. \quad (77)$$

Here  $n_{\text{GPu}}^e$  are the number of Gauss-points in the mechanical element  $e$ ;  $w_u^{e(j)}$  symbolizes the weighting factor of the spatial integration scheme, where we assume a Gauss-integration formula;  $\mathbf{B}_u^{e(j)} = \mathbf{B}_u(\boldsymbol{\xi}^{(j)})$  is the strain-displacement matrix used in (69) and evaluated at Gauss-point  $\boldsymbol{\xi}^{(j)}$ ;  $\mathbf{E}^{e(j)} = \mathbf{E}^e(t, \boldsymbol{\xi}^{(j)}, \mathbf{u})$  are the strains (69);  $\Theta^{e(j)} = \Theta^e(t, \boldsymbol{\xi}^{(j)}, \boldsymbol{\Theta})$  defines the temperature (66); and  $\mathbf{q}^{e(j)} = \mathbf{q}^e(t, \boldsymbol{\xi}^{(j)})$  the internal variables at Gauss-point  $\boldsymbol{\xi}^{(j)}$ . The Jacobian of the coordinate transformation is defined as  $\mathbf{J}_u^{e(j)} = d\boldsymbol{\chi}_u^e(\boldsymbol{\xi})/d\boldsymbol{\xi}|_{\boldsymbol{\xi}=\boldsymbol{\xi}^{(j)}}$  and  $\bar{\mathbf{p}}(t)$  symbolizes the equivalent nodal force vector.

Following [Ellsiepen and Hartmann 2001], we formally assemble all internal variables of all Gauss-points into a large vector

$$\mathbf{q}(t) = \sum_{e=1}^{n_{\text{el}}^u} \sum_{j=1}^{n_{\text{GPu}}^e} \mathbf{Z}_Q^{e(j)T} \mathbf{q}^{e(j)}(t) \quad (\text{or } \mathbf{q}^{e(j)}(t) = \mathbf{Z}_Q^{e(j)} \mathbf{q}(t)), \quad (78)$$

and the ordinary differential equations (evolution equations of the internal variables) are treated in the same manner ( $\mathbf{r}_Q = \sum_{e=1}^{n_{\text{el}}^u} \sum_{j=1}^{n_{\text{GPu}}^e} \mathbf{Z}_Q^{e(j)T} \mathbf{r}_Q(\mathbf{E}^{e(j)}, \Theta^{e(j)}, \mathbf{q}^{e(j)})$ ), which leads to

$$\dot{\mathbf{q}}(t) = \mathbf{r}_Q(t, \mathbf{u}, \boldsymbol{\Theta}, \mathbf{q}). \quad (79)$$

In our case  $\mathbf{q}^{e(j)} \in \mathbb{R}^{n_q}$  with  $n_q = 12$  (symmetry of the tensors  $\mathbf{E}_v$  and  $\mathbf{E}_r$  is assumed),  $\mathbf{Z}_Q^{e(j)} \in \mathbb{R}^{n_q \times n_Q}$ , and  $\mathbf{q} \in \mathbb{R}^{n_Q}$  hold.

In its spatially discretized representation, the weak form of the heat equation (9) reads

$$\mathbf{g}_\Theta(t, \mathbf{u}, \dot{\mathbf{u}}, \boldsymbol{\Theta}, \dot{\boldsymbol{\Theta}}, \mathbf{q}) = \sum_{e=1}^{n_{\text{el}}^\Theta} \mathbf{Z}_\Theta^{eT} \left\{ \sum_{j=1}^{n_{\text{GP}\Theta}^e} w_\Theta^{(j)} \hat{c}_p(\mathbf{E}^{e(j)}, \Theta^{e(j)}) \mathbf{N}_\Theta^{e(j)} \dot{\Theta}^{e(j)}(t) \det \mathbf{J}_\Theta^{e(j)} \right\} + \mathbf{p}_\kappa(t, \boldsymbol{\Theta}) - \bar{\mathbf{p}}_\Theta(t, \boldsymbol{\Theta}) - \hat{\mathbf{p}}_\Theta(t, \mathbf{u}, \dot{\mathbf{u}}, \boldsymbol{\Theta}, \mathbf{q}), \quad (80)$$

or by inserting (66)–(68) and (72), (73) one obtains the more brief form

$$\mathbf{C}_\Theta(t, \mathbf{u}, \boldsymbol{\Theta}) \dot{\boldsymbol{\Theta}}(t) = \mathbf{r}_\Theta(t, \mathbf{u}, \dot{\mathbf{u}}, \boldsymbol{\Theta}, \mathbf{q}). \quad (81)$$

In this equation, the temperature-dependent heat capacity matrix is obtained:

$$\mathbf{C}_\Theta(t, \mathbf{u}, \boldsymbol{\Theta}) = \sum_{e=1}^{n_{\text{el}}^\Theta} \mathbf{Z}_\Theta^{eT} \left[ \sum_{j=1}^{n_{\text{GP}\Theta}^e} w_\Theta^{(j)} \hat{c}_p(\mathbf{E}^{e(j)}, \Theta^{e(j)}) \mathbf{N}_\Theta^{e(j)} \mathbf{N}_\Theta^{e(j)T} \det \mathbf{J}_\Theta^{e(j)} \right] \mathbf{Z}_\Theta^e \quad (82)$$

( $\mathbf{C}_\Theta \in \mathbb{R}^{n_{\Theta u} \times n_{\Theta u}}$ ) and

$$\mathbf{r}_\Theta(t, \mathbf{u}, \dot{\mathbf{u}}, \boldsymbol{\Theta}, \mathbf{q}) = -\mathbf{p}_\kappa(t, \boldsymbol{\Theta}) + \bar{\mathbf{p}}_\Theta(t, \boldsymbol{\Theta}) + \hat{\mathbf{p}}_\Theta(t, \mathbf{u}, \dot{\mathbf{u}}, \boldsymbol{\Theta}, \mathbf{q}), \quad (83)$$

with the conductivity term

$$\mathbf{p}_\kappa(t, \boldsymbol{\Theta}) = \sum_{e=1}^{n_{\text{el}}^\Theta} \mathbf{Z}_\Theta^{eT} \left\{ \sum_{j=1}^{n_{\text{GP}\Theta}^e} w_\Theta^{(j)} \kappa(\Theta^{e(j)}) \mathbf{B}_\Theta^{e(j)T} \boldsymbol{\gamma}^e(\Theta^{e(j)}(t)) \det \mathbf{J}_\Theta^{e(j)} \right\} \quad (84)$$

and the dissipation term

$$\hat{\rho}_{\Theta}(t, \mathbf{u}, \dot{\mathbf{u}}, \Theta, \mathbf{q}) = \sum_{e=1}^{n_{\text{el}}^{\Theta}} \mathbf{z}_{\Theta}^{eT} \left\{ \sum_{j=1}^{n_{\text{GP}\Theta}^e} w_{\Theta}^{(j)} \hat{p}(\mathbf{E}^{e(j)}, \dot{\mathbf{E}}^{e(j)}, \Theta^{e(j)}, \mathbf{q}^{e(j)}) \mathbf{N}_{\Theta}^{e(j)} \det \mathbf{J}_{\Theta}^{e(j)} \right\}. \quad (85)$$

For reasons of brevity, the heat flux and heat source on the surface are not explained in detail:

$$\bar{\mathbf{p}}_{\Theta}(t, \Theta) = \int_A \mathbf{N}_{\Theta} q^h(\Theta^h) dA + \int_V \mathbf{N}_{\Theta} r^h dV. \quad (86)$$

### Appendix B. Time adaptivity

Regarding computational efficiency and accuracy, methods with a constant step-size perform poorly if the solution varies rapidly in some parts of the time interval and slowly in other parts. For this reason the step-size should be chosen in such a way that it is large in smooth parts and small in transient parts. This calls for a step-size control technique which relies on the approximation of the local integration error and adjusts the time-step so that the error measure remains within a prescribed tolerance. Since an adaptive step-size control takes the behavior of the underlying equations into account, it stabilizes the global procedure and keeps the global error within certain limits as well. The first widely used adaptive time-stepping strategies in the field of structural dynamics were proposed in [Zienkiewicz et al. 1984; Zienkiewicz and Xie 1991; Zeng et al. 1992; Li et al. 1993; Riccius and Schweizerhof 1996; Riccius 1997]. These approaches are based on an a posteriori estimation of the local integration error (see (89)) for the displacement field which results from a difference between numerical solution and an improved solution calculated in a Taylor series at  $t_n$ . Further details regarding this a posteriori error estimation technique and specific numerical examples in combination with generalized- $\alpha$  related methods can be found in [Kuhl 1996; Kuhl and Ramm 1999]. An a posteriori error estimation technique for displacements and velocities is proposed in [Hulbert and Jang 1995]. Step-size control algorithms based on the “apparent highest frequency” as well other classical approaches built on general frequency information lie out of our scope. In this section, we focus on the possibility of incorporating an efficient step-size control, which is based on the estimation of the local integration error (local truncation error) and can be achieved with a so-called embedding technique [Hairer et al. 1993; Hairer and Wanner 1996; Strehmel et al. 2012]. A further approach for the time-adaptivity of one-step methods — the Richardson extrapolation — is presented in [Hairer et al. 1993]. Due to the necessity of repeating the time-step with  $\Delta t_n/2$  and comparing the results to the computations with the time-step  $\Delta t_n$ , a higher computational effort is required. For that reason, local error control using the Richardson extrapolation is not of particular interest to us.

We start with recapping the coupled ODE system in (10) in explicit form

$$\dot{\mathbf{y}}(t) = \mathbf{f}(t, \mathbf{y}(t)), \quad \mathbf{y}(t_0) = \mathbf{y}_0, \quad (87)$$

with  $\mathbf{y} = \{\mathbf{u}^T, \mathbf{v}^T, \Theta^T, \mathbf{q}^T\} \in \mathbb{R}^{(2n_{\text{uu}} + n_{\Theta} + n_{\text{Q}})}$ .

Based on an exact value  $\mathbf{y}_n = \mathbf{y}(t_n)$  the local integration error  $\delta$  in the time interval  $\Delta t_n$  is defined by the difference between the exact solution  $\mathbf{y}(t_{n+1})$  and the numerical solution

$$\mathbf{y}_{n+1} = \mathbf{y}(t_n) + \Delta t_n \Phi(t_n, \mathbf{y}(t_n), \Delta t_n), \quad (88)$$

using an arbitrary integration method of order  $p$  as

$$\begin{aligned}\delta &= \mathbf{y}(t_{n+1}) - \mathbf{y}_{n+1} = \mathbf{y}(t_{n+1}) - (\mathbf{y}(t_n) + \Delta t_n \Phi(t_n, \mathbf{y}(t_n), \Delta t_n)) \\ &= \Delta t_n^{p+1} \Psi(t_n, \mathbf{y}) + \mathcal{O}(\Delta t_n^{p+2}).\end{aligned}\quad (89)$$

Here,  $\Phi$  marks the so-called increment function of the underlying integrator [Hairer et al. 1993; Strehmel et al. 2012]. Based on Taylor series expansions of the exact solution and the numerical solution, we can determine the order of consistency where the local truncation error can be split up into a main part  $\Delta t_n^{p+1} \Psi$  (principal error) and a remainder of order  $p + 2$ . In the following, the main part of the local integration error  $\delta$  is estimated so as to be able to control the error quantity. For this purpose, two methods of different order  $p$  and  $\hat{p} = p - 1$  are assumed:

$$\begin{aligned}\mathbf{y}_{n+1} &= \mathbf{y}(t_n) + \Delta t_n \Phi(t_n, \mathbf{y}(t_n), \Delta t_n), \\ \hat{\mathbf{y}}_{n+1} &= \mathbf{y}(t_n) + \Delta t_n \hat{\Phi}(t_n, \mathbf{y}(t_n), \Delta t_n).\end{aligned}\quad (90)$$

Each of these methods yield an expression for the local integration error

$$\begin{aligned}\delta &= \mathbf{y}(t_{n+1}) - \mathbf{y}_{n+1} = \Delta t_n^{p+1} \Psi(t_n, \mathbf{y}) + \mathcal{O}(\Delta t_n^{p+2}), \\ \hat{\delta} &= \mathbf{y}(t_{n+1}) - \hat{\mathbf{y}}_{n+1} = \Delta t_n^{\hat{p}+1} \hat{\Psi}(t_n, \mathbf{y}) + \mathcal{O}(\Delta t_n^{\hat{p}+2}).\end{aligned}\quad (91)$$

Using the difference of both errors

$$\delta - \hat{\delta} = \mathbf{y}_{\text{err}} := \hat{\mathbf{y}}_{n+1} - \mathbf{y}_{n+1} = \Delta t_n^{\hat{p}+1} \hat{\Psi}(t_n, \mathbf{y}) + \mathcal{O}(\Delta t_n^{\hat{p}+2}) \approx \Delta t_n^{\hat{p}+1} \hat{\Psi}(t_n, \mathbf{y}),\quad (92)$$

we are able to estimate the main part  $\Delta t_n^{\hat{p}+1} \hat{\Psi}$  of the local integration error of the lower order method, i.e., we get the “second best” approximation of  $\mathbf{y}(t_{n+1})$ . Furthermore, we assume that the function  $\hat{\Psi}$  varies only slowly so that  $\|\hat{\Psi}(t_n, \mathbf{y})\| \approx C$  holds within  $\Delta t_n$ . With this error estimate in hand we are able to decide whether the error in each time step is lower than a user-specified tolerance

$$\|\mathbf{y}_{\text{err}}\| \approx C \Delta t_n^{\hat{p}+1} \leq \varepsilon_r \|\hat{\mathbf{y}}_n\| + \varepsilon_a,\quad (93)$$

where generally the tolerance value is given as combination of an absolute  $\varepsilon_a$  and a relative  $\varepsilon_r$  tolerance. For the computation of an optimal new step-size  $\Delta t_{\text{new}}$ , we demand that the error equals the prescribed mixed tolerance

$$C \Delta t_{\text{new}}^{\hat{p}+1} = \varepsilon_r \|\hat{\mathbf{y}}_n\| + \varepsilon_a.\quad (94)$$

Eliminating the constant  $C$  by using the relationship in (93) and substituting it into (94), we arrive at the desired result

$$\Delta t_{\text{new}} = \Delta t_n \left( \frac{\varepsilon_r \|\hat{\mathbf{y}}_n\| + \varepsilon_a}{\|\mathbf{y}_{\text{err}}\|} \right)^{1/(\hat{p}+1)}.\quad (95)$$

In the numerical mathematics community it is common to advance the solution in time by using the higher-order approximation  $\mathbf{y}_{n+1}$  instead of  $\hat{\mathbf{y}}_{n+1}$ . We do so as well. The case in which the concept of local error control is slightly abandoned is called *local extrapolation* (see [Hairer et al. 1993] for further explanations). A theoretical justification for this violation is given in [Deuffhard and Bornemann 1994].

For the approximation of the local error in the case of DIRK schemes, we use a highly efficient method which is based on an embedded Runge–Kutta scheme. For this purpose two  $s$ -stage methods of different

$$\begin{array}{c|c}
c & \mathbf{A} \\
\hline
\mathbf{b}^T & \\
\hat{\mathbf{b}}^T &
\end{array}
\qquad
\begin{array}{c|c|c}
c & \bar{\mathbf{A}} & \mathbf{A} \\
\hline
\bar{\mathbf{b}}^T & & \mathbf{b}^T \\
\hat{\mathbf{b}}^T & & \hat{\mathbf{b}}^T
\end{array}$$

**Figure 17.** Butcher-tableaus with embedding: embedded RK scheme (left) and embedded RKN scheme (right).

order  $p$  and  $\hat{p}$  are constructed with identical stages  $c_i$ , the same coefficient matrix  $\mathbf{A}$ , but using different weighting factors  $b_i$  and  $\hat{b}_i$ . The pair of embedded RK methods share the same stage computations. Thus, a further solution at  $t_{n+1}$  can be computed by using (29), (25)<sub>2</sub>–(25)<sub>4</sub>

$$\begin{aligned}
\hat{\mathbf{u}}_{n+1} &= \mathbf{u}_n + \Delta t_n \mathbf{v}_n + \Delta t_n^2 \sum_{i=1}^s \hat{b}_i \mathbf{A}_{ni}, & \hat{\mathbf{v}}_{n+1} &= \mathbf{v}_n + \Delta t_n \sum_{i=1}^s \hat{b}_i \mathbf{A}_{ni}, \\
\hat{\Theta}_{n+1} &= \Theta_n + \Delta t_n \sum_{i=1}^s \hat{b}_i \dot{\Theta}_{ni}, & \hat{\mathbf{q}}_{n+1} &= \mathbf{q}_n + \Delta t_n \sum_{i=1}^s \hat{b}_i \dot{\mathbf{Q}}_{ni},
\end{aligned} \tag{96}$$

with the newly introduced algorithmic parameters  $\hat{b}_i$  and  $\hat{\hat{b}}_i = \sum_{j=1}^s \hat{b}_j a_{ji}$ . As in [Ehlers and Ellsiepen 1998; Diebels et al. 1999], we decompose  $\mathbf{y}_{\text{err}}$  into the local integration error for each field variable in order to take the different physical properties and the order of magnitude into account. Commonly, the new weighting factors  $\hat{b}_i$  and  $\hat{\hat{b}}_i$  are appended to the Butcher array to form an embedded RK scheme (see Figure 17).

The consistency orders of the two methods differ by one (i.e.,  $\hat{p} = p - 1$ ). According to (92), a simple hand calculation results in the following estimation formula for RK schemes:

$$\begin{aligned}
\mathbf{u}_{\text{err}} &= \hat{\mathbf{u}}_{n+1} - \mathbf{u}_{n+1} = \Delta t_n^2 \sum_{i=1}^s (\hat{b}_i - \bar{b}_i) \mathbf{A}_{ni}, & \mathbf{v}_{\text{err}} &= \hat{\mathbf{v}}_{n+1} - \mathbf{v}_{n+1} = \Delta t_n \sum_{i=1}^s (\hat{b}_i - b_i) \mathbf{A}_{ni}, \\
\Theta_{\text{err}} &= \hat{\Theta}_{n+1} - \Theta_{n+1} = \Delta t_n \sum_{i=1}^s (\hat{b}_i - b_i) \dot{\Theta}_{ni}, & \mathbf{q}_{\text{err}} &= \hat{\mathbf{q}}_{n+1} - \mathbf{q}_{n+1} = \Delta t_n \sum_{i=1}^s (\hat{b}_i - b_i) \dot{\mathbf{Q}}_{ni},
\end{aligned} \tag{97}$$

where the stage derivatives of both integration schemes are equal on the basis of the same coefficients  $a_{ij}$  and  $\bar{a}_{ij}$ .

In the case of the generalized- $\alpha$  method we follow a proposal in [Rang 2013a]. There, the approximation of the generalized- $\alpha$  scheme was used as a second-order approximation ( $p = 2$ ) since the error constant is very small and since the methods in our numerical experiments (see Section 4) behave as a second-order method [Chung and Hulbert 1993; Erlicher et al. 2002; Rang 2013a]. The Backward Euler method can be used for a second solution of lower order  $\hat{p} = 1$ . To circumvent an entire calculation of (10) by using the Backward Euler method, the necessary derivatives will be approximated by using (38), (39), (46) and (54). The computation for the local truncation error quantities in each field variable yield

$$\begin{aligned}
\mathbf{u}_{\text{err}} &= \hat{\mathbf{u}}_{n+1} - \mathbf{u}_{n+1} = \mathbf{u}_n + \Delta t_n \mathbf{v}_{n+1} - \mathbf{u}_{n+1}, & \mathbf{v}_{\text{err}} &= \hat{\mathbf{v}}_{n+1} - \mathbf{v}_{n+1} = \mathbf{v}_n + \Delta t_n \mathbf{a}_{n+1} - \mathbf{v}_{n+1}, \\
\Theta_{\text{err}} &= \hat{\Theta}_{n+1} - \Theta_{n+1} = \Theta_n + \Delta t_n \dot{\Theta}_{n+1} - \Theta_{n+1}, & \mathbf{q}_{\text{err}} &= \hat{\mathbf{q}}_{n+1} - \mathbf{q}_{n+1} = \mathbf{q}_n + \Delta t_n \dot{\mathbf{q}}_{n+1} - \mathbf{q}_{n+1}.
\end{aligned} \tag{98}$$

Commonly, the estimation of  $\Delta t_{\text{new}}$  is carried out using a more efficient and computationally more stable procedure if it is described by (95). Following the proposal in [Hairer et al. 1993; Hairer and Wanner 1996; Gustafsson 1994], we employ the relative error measures

$$\begin{aligned} e_u &:= \sqrt{\frac{1}{n_{\text{uu}}} \sum_{k=1}^{n_{\text{uu}}} \left( \frac{u_{\text{err}}^k}{\varepsilon_r^u |u_n^k| + \varepsilon_a^u} \right)^2}, & e_v &:= \sqrt{\frac{1}{n_{\text{uu}}} \sum_{k=1}^{n_{\text{uu}}} \left( \frac{v_{\text{err}}^k}{\varepsilon_r^v |v_n^k| + \varepsilon_a^v} \right)^2}, \\ e_{\Theta} &:= \sqrt{\frac{1}{n_{\Theta u}} \sum_{k=1}^{n_{\Theta u}} \left( \frac{\Theta_{\text{err}}^k}{\varepsilon_r^{\Theta} |\Theta_n^k| + \varepsilon_a^{\Theta}} \right)^2}, \end{aligned} \quad (99)$$

where  $u_{\text{err}}^k$ ,  $v_{\text{err}}^k$  and  $\Theta_{\text{err}}^k$  are the  $k$ -th components of the local integration error approximations  $\mathbf{u}_{\text{err}}$ ,  $\mathbf{v}_{\text{err}}$ ,  $\Theta_{\text{err}}$ , respectively. These error measures perform a componentwise weighting instead of the simple global weighting  $\|\mathbf{y}_{\text{err}}\|/(\varepsilon_r \|\mathbf{y}_n\| + \varepsilon_a)$  introduced in (94). For the local truncation error  $\mathbf{q}_{\text{err}}$  in the interval variables, Diebels et al. [1999] proposed the maximum norm

$$e_q := \max_{1 \leq k \leq n_Q} \left| \frac{q_{\text{err}}^k}{\varepsilon_r^q |q_n^k| + \varepsilon_a^q} \right|. \quad (100)$$

Furthermore, the user-defined relative  $\varepsilon_r^u$ ,  $\varepsilon_r^v$ ,  $\varepsilon_r^{\Theta}$ ,  $\varepsilon_r^q$  and absolute  $\varepsilon_a^u$ ,  $\varepsilon_a^v$ ,  $\varepsilon_a^{\Theta}$ ,  $\varepsilon_a^q$  error tolerances may depend on the components of the field variables reflecting different magnitude and physical meaning of these quantities [Hairer et al. 1993]. For the sake of simplicity they are chosen to be constant. The maximum  $e_m = \max(e_u, e_v, e_{\Theta}, e_q)$  of the weighted error measures is used to determine the new step-size,

$$\Delta t_{\text{new}} = \Delta t_n \cdot \begin{cases} \max(f_{\min}, f_{\text{safety}} e_m^{-1/(\hat{p}+1)}) & \text{if } e_m > 1 \\ \min(f_{\max}, f_{\text{safety}} e_m^{-1/(\hat{p}+1)}) & \text{if } e_m \leq 1 \end{cases}, \quad (101)$$

comparing  $e_m$  to one. In the case  $e_m \leq 1$  the computed step is accepted and the integration can march forward with  $\Delta t_{\text{new}}$ , otherwise the step has to be repeated with a smaller step-size  $\Delta t_{\text{new}}$ . The safety factor  $0 < f_{\text{safety}} < 1$  prevents oscillations in the step-size controller while  $f_{\min}$  and  $f_{\max}$  keep the step-size from increasing and decreasing too fast. In practice, typical values for these factors are:  $0.8 \leq f_{\text{safety}} \leq 0.9$ ,  $0.2 \leq f_{\min} \leq 0.5$ ,  $2 \leq f_{\max} \leq 3$  [Ellsiepen and Hartmann 2001].

Although the proposed standard controller [Hairer et al. 1993] works quite well, the local error control algorithm yields strong oscillations in the step-size behavior in phases of quickly changing dynamics [Gustafsson et al. 1988; Gustafsson 1991; 1994; Strehmel et al. 2012]. With regard to a further stabilization and an increased time integration performance of the step-size controller, several approaches from a control theoretical point of view were studied in [Gustafsson et al. 1988; Gustafsson 1991; 1994; Söderlind 2002]. In Section 4 we employ a modified hybrid PI-controller based on [Lang 2001], which works according to the following step-size selection rule

$$\Delta t_{\text{new}} = \Delta t_n \cdot \begin{cases} \min(f_{\max}, \max(f_{\min}, f_{\text{safety}} (1/e_m^{n+1})^{K_I} (e_m^n/e_m^{n+1})^{K_P})) & \text{if } e_m > 1 \\ \min(f_{\max}, \max(f_{\min}, f_{\text{safety}} (1/e_m^{n+1})^{K_I})) & \text{if } e_m \leq 1 \end{cases}, \quad (102)$$

using time-step and error data  $e_m^n$  from the previous time-step.  $K_P$  and  $K_I$  define the proportional and the integral gain of the controller, which can also be dependent on previous time-steps sizes and on



previously computed error data. For further details about the implementation of the proposed automatic step-length control we refer to [Gustafsson 1994; Hairer and Wanner 1996; Lang 2001].

## References

- [Alexander 1977] R. Alexander, “Diagonally implicit Runge–Kutta methods for stiff ODE’s”, *SIAM J. Numer. Anal.* **14**:6 (1977), 1006–1021.
- [Armero and Simo 1992] F. Armero and J. C. Simo, “A new unconditionally stable fractional step method for nonlinear coupled thermomechanical problems”, *Internat. J. Numer. Methods Eng.* **35**:4 (1992), 737–766.
- [Armero and Simo 1993] F. Armero and J. C. Simo, “A priori stability estimates and unconditionally stable product formula algorithms for nonlinear coupled thermoplasticity”, *Int. J. Plasticity* **9**:6 (1993), 749–782.
- [Belytschko et al. 2000] T. Belytschko, W. K. Liu, and B. Moran, *Nonlinear finite elements for continua and structures*, Wiley, Chichester, England, 2000.
- [Birken et al. 2010] P. Birken, K. J. Quint, S. Hartmann, and A. Meister, “A time-adaptive fluid-structure interaction method for thermal coupling”, *Comput. Vis. Sci.* **13**:7 (2010), 331–340.
- [Butcher 2008] J. C. Butcher, *Numerical methods for ordinary differential equations*, 2nd ed., Wiley, Chichester, England, 2008.
- [Cash 1979] J. Cash, “Diagonally implicit Runge–Kutta formulae with error estimates”, *J. Inst. Math. Appl.* **24** (1979), 293–301.
- [Chung and Hulbert 1993] J. Chung and G. M. Hulbert, “A time integration algorithm for structural dynamics with improved numerical dissipation: the generalized- $\alpha$  method”, *Trans. ASME J. Appl. Mech.* **60**:2 (1993), 371–375.
- [Conde Martín et al. 2014] S. Conde Martín, J. C. García Orden, and I. Romero, “Energy-consistent time integration for nonlinear viscoelasticity”, *Comput. Mech.* **54**:2 (2014), 473–488.
- [Dettmer and Perić 2003] W. Dettmer and D. Perić, “An analysis of the time integration algorithms for the finite element solutions of incompressible Navier–Stokes equations based on a stabilised formulation”, *Comput. Methods Appl. Mech. Eng.* **192**:9–10 (2003), 1177–1226.
- [Deuffhard and Bornemann 1994] P. Deuffhard and F. Bornemann, *Numerische Mathematik II: Integration gewöhnlicher Differentialgleichungen*, Walter de Gruyter & Co., Berlin, 1994.
- [Diebels et al. 1999] S. Diebels, P. Ellsiepen, and W. Ehlers, “Error-controlled Runge–Kutta Time Integration of a Viscoplastic Hybrid Two-phases Model”, *Technische Mechanik* **19** (1999), 19–27.
- [Ehlers and Ellsiepen 1998] W. Ehlers and P. Ellsiepen, “Adaptive Zeitintegration–Verfahren für ein elastisch-viskoplastisches Zweiphasenmodell”, *ZAMM Zeitschrift für Angewandte Mathematik und Mechanik* **78** (1998), S361–S362.
- [Ellsiepen 1999] P. Ellsiepen, *Zeit- und ortsadaptive Verfahren angewandt auf Mehrphasenprobleme poröser Medien*, Doctoral Thesis, Institute of Mechanics II, University of Stuttgart, 1999.
- [Ellsiepen and Hartmann 2001] P. Ellsiepen and S. Hartmann, “Remarks on the interpretation of current non-linear finite-element-analyses as differential-algebraic equations”, *Int. J. Numer. Meth. Eng.* **51** (2001), 679–707.
- [Erbs and Düster 2012] P. Erbs and A. Düster, “Accelerated staggered coupling schemes for problems of thermoelasticity at finite strains”, *Comput. Math. Appl.* **64**:8 (2012), 2408–2430.
- [Erbs et al. 2015] P. Erbs, S. Hartmann, and A. Düster, “A partitioned solution approach for electro-thermo-mechanical problems”, *Archive of Applied Mechanics* **85**:8 (2015), 1075–1101.
- [Erlicher et al. 2002] S. Erlicher, L. Bonaventura, and O. S. Bursi, “The analysis of the generalized- $\alpha$  method for non-linear dynamic problems”, *Comput. Mech.* **28**:2 (2002), 83–104.
- [Felippa and Park 1980] C. Felippa and K. Park, “Staggered transient analysis procedures for coupled mechanical systems: formulation”, *Comput. Methods Appl. Mech. Eng.* **24** (1980), 61–111.
- [Felippa et al. 2001] C. A. Felippa, K. Park, and C. Farhat, “Partitioned analysis of coupled mechanical systems”, *Comput. Methods Appl. Mech. Eng.* **190**:24–25 (2001), 3247–3270.

- [Fritzen 1997] P. Fritzen, *Numerische behandlung nichtlinearer probleme der elastizitäts- und plastizitätstheorie*, Ph.D. thesis, Universität Darmstadt, 1997.
- [Gear 1986] C. W. Gear, “Maintaining solution invariants in the numerical solution of ODEs”, *SIAM J. Sci. Statist. Comput.* **7**:3 (1986), 734–743.
- [Glaser 1991] S. Glaser, “Berechnung gekoppelter thermomechanischer Prozesse”, Institut für Statik und Dynamik der Luft- und Raumfahrtkonstruktionen, Universität Stuttgart, Stuttgart (Germany), 1991.
- [Gonzalez 2000] O. Gonzalez, “Exact energy and momentum conserving algorithms for general models in nonlinear elasticity”, *Comput. Methods Appl. Mech. Eng.* **190**:13-14 (2000), 1763–1783.
- [Gustafsson 1991] K. Gustafsson, “Control-theoretic techniques for stepsize selection in explicit Runge–Kutta methods”, *ACM Trans. Math. Software* **17**:4 (1991), 533–554.
- [Gustafsson 1994] K. Gustafsson, “Control-theoretic techniques for stepsize selection in implicit Runge–Kutta methods”, *ACM Trans. Math. Software* **20**:4 (1994), 496–517.
- [Gustafsson et al. 1988] K. Gustafsson, M. Lundh, and G. Söderlind, “A PI stepsize control for the numerical solution of ordinary differential equations”, *BIT* **28**:2 (1988), 270–287.
- [Hairer and Wanner 1996] E. Hairer and G. Wanner, *Solving ordinary differential equations II*, 2nd ed., Springer Series in Computational Mathematics **14**, Springer, Berlin, 1996.
- [Hairer et al. 1989] E. Hairer, C. Lubich, and M. Roche, *The numerical solution of differential-algebraic systems by Runge–Kutta methods*, Lecture Notes in Mathematics **1409**, Springer, Berlin, 1989.
- [Hairer et al. 1993] E. Hairer, S. P. Nørsett, and G. Wanner, *Solving ordinary differential equations I*, 2nd ed., Springer Series in Computational Mathematics **8**, Springer, Berlin, 1993.
- [Hamkar 2013] A.-W. Hamkar, *Eine iterationsfreie finite-elemente methode im Rahmen der finiten thermoviskoelastizität*, Ph.D. thesis, Report No. 1/2013, Institute of Applied Mechanics, Clausthal University of Technology, Clausthal-Zellerfeld, 2013.
- [Hartmann 2002] S. Hartmann, “Computation in finite-strain viscoelasticity: finite elements based on the interpretation as differential-algebraic equations”, *Comput. Methods Appl. Mech. Eng.* **191**:13-14 (2002), 1439–1470.
- [Hartmann 2005] S. Hartmann, “A remark on the application of the Newton–Raphson method in non-linear finite element analysis”, *Comput. Mech.* **36**:2 (2005), 100–116.
- [Hartmann 2007] S. Hartmann, *Kontaktanalyse dünnwandiger Strukturen bei großen Deformationen*, Ph.D. thesis, Universität Stuttgart, 2007, Available at <http://elib.uni-stuttgart.de/opus/volltexte/2007/3109/>.
- [Hartmann and Hamkar 2010] S. Hartmann and A.-W. Hamkar, “Rosenbrock-type methods applied to finite element computations within finite strain viscoelasticity”, *Comput. Methods Appl. Mech. Eng.* **199**:23-24 (2010), 1455–1470.
- [Hartmann and Rothe 2013] S. Hartmann and S. Rothe, “A rigorous application of the method of vertical lines to coupled systems in finite element analysis”, pp. 161–175 in *Recent developments in the numerics of nonlinear hyperbolic conservation laws*, edited by R. Ansgore et al., Notes Numer. Fluid Mech. Multidiscip. Des. **120**, Springer, Heidelberg, Germany, 2013.
- [Hartmann et al. 2008a] S. Hartmann, K. J. Quint, and M. Arnold, “On plastic incompressibility within time-adaptive finite elements combined with projection techniques”, *Comput. Methods Appl. Mech. Eng.* **198**:2 (2008), 178–193.
- [Hartmann et al. 2008b] S. Hartmann, K. J. Quint, and A.-W. Hamkar, “Displacement control in time-adaptive non-linear finite-element analysis”, *ZAMM Z. Angew. Math. Mech.* **88**:5 (2008), 342–364.
- [Hilber et al. 1977] H. M. Hilber, T. J. R. Hughes, and R. L. Taylor, “Improved numerical dissipation for time integration algorithms in structural dynamics”, *Earthquake Eng. Struct.* **5**:3 (1977), 283–292.
- [Hughes 1987] T. J. R. Hughes, *The finite element method*, Prentice Hall, Englewood Cliffs, New Jersey, 1987.
- [Hulbert and Jang 1995] G. M. Hulbert and I. Jang, “Automatic time step control algorithms for structural dynamics”, *Comput. Methods Appl. Mech. Eng.* **126**:1-2 (1995), 155–178.
- [Jansen et al. 2000] K. E. Jansen, C. H. Whiting, and G. M. Hulbert, “A generalized- $\alpha$  method for integrating the filtered Navier–Stokes equations with a stabilized finite element method”, *Comput. Methods Appl. Mech. Eng.* **190**:3-4 (2000), 305–319.
- [Kreisselmeier and Steinhauser 1979] G. Kreisselmeier and R. Steinhauser, “Systematische Auslegung von Reglern durch Optimierung eines vektoriiellen Gütekriteriums”, *Regelungstechnik* **3** (1979), 76–79.

- [Krüger et al. 2016] M. Krüger, M. Groß, and P. Betsch, “An energy-entropy-consistent time stepping scheme for nonlinear thermo-viscoelastic continua”, *ZAMM Z. Angew. Math. Mech.* **96**:2 (2016), 141–178.
- [Kuhl 1996] D. Kuhl, *Stabile Zeitintegrationsalgorithmen in der nichtlinearen Elastodynamik dünnwandiger Tragwerke*, PhD-thesis, Report No. 2 (1996), University of Stuttgart (Germany), Institute for Structural Mechanics, 1996.
- [Kuhl and Crisfield 1999] D. Kuhl and M. A. Crisfield, “Energy-conserving and decaying algorithms in non-linear structural dynamics”, *Int. J. Numer. Methods Eng.* **45**:5 (1999), 569–599.
- [Kuhl and Ramm 1999] D. Kuhl and E. Ramm, “Generalized energy-momentum method for non-linear adaptive shell dynamics”, *Comput. Methods Appl. Mech. Eng.* **178**:3-4 (1999), 343–366.
- [Lang 2001] J. Lang, *Adaptive multilevel solution of nonlinear parabolic PDE systems*, Lecture Notes in Computational Science and Engineering **16**, Springer, Berlin, 2001.
- [Lewis et al. 1996] R. W. Lewis, K. Morgan, H. R. Thomas, and K. N. Seetharamu, *The finite element method in heat transfer analysis*, Wiley, 1996.
- [Li et al. 1993] X. Li, L. Zeng, and N.-E. Wiberg, “A simple local error estimator and an adaptive time-stepping procedure for direct integration method in dynamic analysis”, *Commun. Numer. Methods Eng.* **9**:4 (1993), 273–292.
- [Miehe 1988] C. Miehe, *Zur numerischen Behandlung thermomechanischer Prozesse*, Report No. F88/6, University of Hannover, Institut für Baumechanik und Numerische Mechanik, 1988.
- [Netz and Hartmann 2015] T. Netz and S. Hartmann, “A monolithic finite element approach using high-order schemes in time and space applied to finite strain thermo-viscoelasticity”, *Comput. Math. Appl.* **70**:7 (2015), 1457–1480.
- [Newmark 1959] N. M. Newmark, “A method of computation for structural dynamics”, *J. Eng. Mech. Div. (ASCE)* **85** (1959), 67–94.
- [Noels et al. 2006] L. Noels, L. Stainier, and J.-P. Ponthot, “An energy momentum conserving algorithm using the variational formulation of visco-plastic updates”, *Int. J. Numer. Methods Eng.* **65**:6 (2006), 904–942.
- [Noels et al. 2008] L. Noels, L. Stainier, and J.-P. Ponthot, “A first-order energy-dissipative momentum-conserving scheme for elasto-plasticity using the variational updates formulation”, *Comput. Methods Appl. Mech. Eng.* **197**:6-8 (2008), 706–726.
- [Ortiz and Popov 1985] M. Ortiz and E. P. Popov, “Accuracy and stability of integration algorithms for elastoplastic constitutive relations”, *Int. J. Numer. Methods Eng.* **21**:9 (1985), 1561–1576.
- [Popp 2012] A. Popp, *Mortar methods for computational contact mechanics and general interface problems*, Ph.D. thesis, Technische Universität München, Institute for Computational Mechanics, 2012.
- [Prothero and Robinson 1974] A. Prothero and A. Robinson, “On the stability and accuracy of one-step methods for solving stiff systems of ordinary differential equations”, *Math. Comp.* **28** (1974), 145–162.
- [Quint 2012] K. J. Quint, *Thermomechanically coupled processes for functionally graded materials: experiments, modelling, and finite element analysis using high-order DIRK-methods*, PhD-thesis, Report No. 2/2012, Institute of Applied Mechanics, Clausthal University of Technology, Clausthal-Zellerfeld, 2012.
- [Quint et al. 2011] K. J. Quint, S. Hartmann, S. Rothe, N. Saba, and K. Steinhoff, “Experimental validation of high-order time integration for non-linear heat transfer problems”, *Comput. Mech.* **48**:1 (2011), 81–96.
- [Rabbat et al. 1979] N. Rabbat, A. L. Sangiovanni-Vincentelli, and H. Y. Hsieh, “A multilevel Newton algorithm with macro-modeling and latency for the analysis of large-scale nonlinear circuits in the time domain”, *IEEE Trans. Circuits Syst.* **26** (1979), 733–741.
- [Rang 2013a] J. Rang, “Adaptive timestep control for the generalised- $\alpha$  method”, pp. 559–570 in *Adaptive Modeling and Simulation*, edited by D. Aubry et al., 2013.
- [Rang 2013b] J. Rang, “Coupling generalised- $\alpha$  methods: analysis, adaptivity, and numerics”, pp. 399–410 in *Computational methods for coupled problems in science and engineering V: a conference celebrating the 60th birthday of Eugenio Oñate* (Santa Eulalia, Ibiza, Spain), edited by S. Idelsohn et al., Barcelona, 2013.
- [Reddy and Gartling 2000] J. Reddy and D. K. Gartling, *The finite element method in heat transfer and fluid dynamics*, 2nd ed., CRC Press, Boca Raton, Florida, 2000.
- [Riccius 1997] J. Riccius, *Adaptive Methoden zur statischen und dynamischen Analyse von Flächentragwerken mit linearen Finiten Elementen*, Ph.D. thesis, Institute of Engineering Mechanics, University of Karlsruhe, 1997.

- [Riccius and Schweizerhof 1996] J. Riccius and K. Schweizerhof, “Aspects of hierarchical h-adaptive dynamic analysis”, pp. 61–70 in *Advances in Finite Element Techniques*, edited by B. H. V. Topping, Civil-Comp Press, Edinburgh, Scotland, 1996.
- [Rothe 2015] S. Rothe, *Electro-thermo-mechanical modeling of field assisted sintering technology: experiments, constitutive modeling and finite element analysis*, PhD-thesis, Report No. 1/2015, Institute of Applied Mechanics, Clausthal University of Technology, Clausthal-Zellerfeld, 2015.
- [Rothe et al. 2015a] S. Rothe, P. Erbts, A. Düster, and S. Hartmann, “Monolithic and partitioned coupling schemes for thermo-viscoplasticity”, *Comput. Methods Appl. Mech. Eng.* **293** (2015), 375–410.
- [Rothe et al. 2015b] S. Rothe, J. H. Schmidt, and S. Hartmann, “Analytical and numerical treatment of electro-thermo-mechanical coupling”, *Archive of Applied Mechanics* **85**:9 (2015), 1245–1264.
- [Schrefler 2004] B. A. Schrefler, *Encyclopedia of computational mechanics: multifield problems*, vol. 2, Chapter 17, pp. 575–603, Wiley, Chichester, England, 2004.
- [Simo and Miehe 1992] J. Simo and C. Miehe, “Associative coupled thermoplasticity at finite strains: formulation, numerical analysis and implementation”, *Comput. Methods Appl. Mech. Eng.* **98**:1 (1992), 41–104.
- [Simo and Tarnow 1992] J. C. Simo and N. Tarnow, “The discrete energy-momentum method. Conserving algorithms for nonlinear elastodynamics”, *Z. Angew. Math. Phys.* **43**:5 (1992), 757–792.
- [Simo et al. 1992] J. C. Simo, N. Tarnow, and K. K. Wong, “Exact energy-momentum conserving algorithms and symplectic schemes for nonlinear dynamics”, *Comput. Methods Appl. Mech. Eng.* **100**:1 (1992), 63–116.
- [Söderlind 2002] G. Söderlind, “Automatic control and adaptive time-stepping”, *Numer. Algorithms* **31**:1-4 (2002), 281–310.
- [Strehmel et al. 2012] K. Strehmel, R. Weiner, and H. Podhaisky, *Numerik gewöhnlicher differentialgleichungen*, 2nd ed., Vieweg + Teubner Verlag, Wiesbaden, Germany, 2012.
- [Tsakmakis and Willuweit 2004] C. Tsakmakis and A. Willuweit, “A comparative study of kinematic hardening rules at finite deformations”, *Int. J. Non-Linear Mech.* **39**:4 (2004), 539–554.
- [Wendt et al. 2015] G. Wendt, P. Erbts, and A. Düster, “Partitioned coupling strategies for multi-physically coupled radiative heat transfer problems”, *J. Comput. Phys.* **300** (2015), 327–351.
- [Wood et al. 1980] W. L. Wood, M. Bossak, and O. C. Zienkiewicz, “An alpha modification of Newmark’s method”, *Internat. J. Numer. Methods Eng.* **15**:10 (1980), 1562–1566.
- [Wriggers 2001] P. Wriggers, *Nichtlineare finite-elemente Methoden*, Springer, Berlin, 2001.
- [Zeng et al. 1992] L. F. Zeng, N.-E. Wiberg, X. D. Li, and Y. M. Xie, “A posteriori local error estimation and adaptive time-stepping for newmark integration in dynamic analysis”, *Earthquake Eng. Struct.* **21**:7 (1992), 555–571.
- [Zienkiewicz and Taylor 2000] O. C. Zienkiewicz and R. L. Taylor, *The finite element method*, vol. 2, 5th ed., Butterworth-Heinemann, Oxford, England, 2000.
- [Zienkiewicz and Xie 1991] O. C. Zienkiewicz and Y. M. Xie, “A simple error estimator and adaptive time stepping procedure for dynamic analysis”, *Earthquake Eng. Struct.* **20**:9 (1991), 871–887.
- [Zienkiewicz et al. 1984] O. C. Zienkiewicz, W. L. Wood, N. W. Hine, and R. L. Taylor, “A unified set of single step algorithms I: General formulation and applications”, *Internat. J. Numer. Methods Eng.* **20**:8 (1984), 1529–1552.

Received 28 Feb 2016. Revised 21 May 2016. Accepted 13 Jun 2016.

MATTHIAS GRAFENHORST: [matthias.grafenhorst@tu-clausthal.de](mailto:matthias.grafenhorst@tu-clausthal.de)

*Institute of Applied Mechanics, Clausthal University of Technology, Adolph-Roemer-sträÙe 2A, D-38678 Clausthal-Zellerfeld, Germany*

JOACHIM RANG: [j.rang@tu-bs.de](mailto:j.rang@tu-bs.de)

*Institute of Scientific Computing, Technical University Braunschweig, Hans-Sommer-Str. 65, D-38106 Braunschweig, Germany*

STEFAN HARTMANN: [stefan.hartmann@tu-clausthal.de](mailto:stefan.hartmann@tu-clausthal.de)

*Institute of Applied Mechanics, Clausthal University of Technology, Adolph-Roemer-StraÙe 2A, D-38678 Clausthal-Zellerfeld, Germany*

# JOURNAL OF MECHANICS OF MATERIALS AND STRUCTURES

[msp.org/jomms](http://msp.org/jomms)

Founded by Charles R. Steele and Marie-Louise Steele

## EDITORIAL BOARD

ADAIR R. AGUIAR	University of São Paulo at São Carlos, Brazil
KATIA BERTOLDI	Harvard University, USA
DAVIDE BIGONI	University of Trento, Italy
YIBIN FU	Keele University, UK
IWONA JASIUK	University of Illinois at Urbana-Champaign, USA
C. W. LIM	City University of Hong Kong
THOMAS J. PENCE	Michigan State University, USA
GIANNI ROYER-CARFAGNI	Università degli studi di Parma, Italy
DAVID STEIGMANN	University of California at Berkeley, USA
PAUL STEINMANN	Friedrich-Alexander-Universität Erlangen-Nürnberg, Germany

## ADVISORY BOARD

J. P. CARTER	University of Sydney, Australia
D. H. HODGES	Georgia Institute of Technology, USA
J. HUTCHINSON	Harvard University, USA
D. PAMPLONA	Universidade Católica do Rio de Janeiro, Brazil
M. B. RUBIN	Technion, Haifa, Israel

**PRODUCTION** [production@msp.org](mailto:production@msp.org)

SILVIO LEVY Scientific Editor

---

Cover photo: Ev Shafir

See [msp.org/jomms](http://msp.org/jomms) for submission guidelines.


---

JoMMS (ISSN 1559-3959) at Mathematical Sciences Publishers, 798 Evans Hall #6840, c/o University of California, Berkeley, CA 94720-3840, is published in 10 issues a year. The subscription price for 2017 is US \$615/year for the electronic version, and \$775/year (+\$60, if shipping outside the US) for print and electronic. Subscriptions, requests for back issues, and changes of address should be sent to MSP.

---

JoMMS peer-review and production is managed by EditFLOW<sup>®</sup> from Mathematical Sciences Publishers.

PUBLISHED BY

 **mathematical sciences publishers**  
nonprofit scientific publishing

<http://msp.org/>

© 2017 Mathematical Sciences Publishers

**Special issue on  
Coupled Field Problems  
and Multiphase Materials**

<b>Preface</b>	<b>CORINA S. DRAPACA, STEFAN HARTMANN, JACEK LESZCZYŃSKI, SIVABAL SIVALOGANATHAN and WOJCIECH SUMELKA</b>	<b>1</b>
<b>Variational methods for the solution of fractional discrete/continuous Sturm–Liouville problems</b>	<b>RICARDO ALMEIDA, AGNIESZKA B. MALINOWSKA, M. LUÍSA MORGADO and TATIANA ODZIJEWICZ</b>	<b>3</b>
<b>Analytical and numerical solution of the fractional Euler–Bernoulli beam equation</b>	<b>TOMASZ BLASZCZYK</b>	<b>23</b>
<b>Fractional calculus in neuronal electromechanics</b>	<b>CORINA S. DRAPACA</b>	<b>35</b>
<b>Time-adaptive finite element simulations of dynamical problems for temperature-dependent materials</b>	<b>MATTHIAS GRAFENHORST, JOACHIM RANG and STEFAN HARTMANN</b>	<b>57</b>
<b>Computer simulation of the effective viscosity in Brinkman filtration equation using the Trefftz method</b>	<b>JAN ADAM KOŁODZIEJ, MAGDALENA MIERZWICZAK and JAKUB KRZYSZTOF GRABSKI</b>	<b>93</b>
<b>Numerical simulations of mechanical properties of alumina foams based on computed tomography</b>	<b>ZDZISŁAW NOWAK, MARCIN NOWAK, RYSZARD PEŁCHERSKI, MAREK POTOCZEK and ROMANA ŚLIWA</b>	<b>107</b>
<b>Gradient-enhanced large strain thermoplasticity with automatic linearization and localization simulations</b>	<b>JERZY PAMIN, BALBINA WCISŁO and KATARZYNA KOWALCZYK-GAJEWSKA</b>	<b>123</b>